Causes of missing snowmelt following drought

Dana A Lapides[1,2], W Jesse Hahm[2], Daniella M Rempe[3], John Whiting[1], David N Dralle[1]

[1]Pacific Southwest Research Station, USDA Forest Service, Davis, CA, USA
[2]Department of Geography, Simon Fraser University, Burnaby, BC, Canada
[3]University of Texas, Austin, Austin, TX, USA

This pre-print is not peer-reviewed. This pre-print was submitted to *Geophysical Research Letters.*

Causes of missing snowmelt following drought

Dana A Lapides[1,2], W Jesse Hahm[2], Daniella M Rempe[3], John Whiting[1], David N Dralle[1]

[1]Pacific Southwest Research Station, United States Forest Service, Davis, CA, USA
[2]Department of Geography, Simon Fraser University, Burnaby, BC, Canada
[3]University of Texas, Austin, Austin, TX, USA

Key Points:

- At 15 watersheds in the Sierra Nevada, the root-zone storage deficit explains anomalously low streamflow from snowpack following drought.
- Median error in 2021 predictions is reduced from 60% to 20% by including the deficit in the forecasting model.
- Future drought related perturbations to runoff could be assessed using root-zone storage deficits inferred from distributed hydrologic data.

Corresponding author: Dana A Lapides, `dlapides@sfu.ca`

Abstract

Water management in snowy mountainous regions hinges on forecasting snowmelt runoff. However, droughts are altering snowpack-runoff relationships with ongoing debate about the driving mechanisms. For example, in 2021 in California, less than half of predicted streamflow arrived. Mechanisms proposed for this 'missing' streamflow included changes in evapotranspiration, rainfall, and subsurface moisture conditions. Here, we demonstrate that evapotranspiration in drought years generates dry subsurface conditions that reduce runoff in subsequent years. A model including this legacy of depleted moisture storage reduced median error in 2021 forecasts from 60% to 20% at 15 minimally disturbed basins and from 18% to 2% at 6 water supply basins in the Sierra Nevada (basins range in area from 5-23,051 km^2 and mean annual precipitation from 814-1549 mm. Our findings indicate that the relationship between snowpack and runoff will evolve as plant ecosystems respond to climate change and alter subsurface water storage dynamics.

Plain Language Summary

Essential water supply from snowpack may become more difficult to predict as the climate changes. Following a recent drought in California, the traditionally used model for snowmelt runoff failed. Here, we present a model that accounts for this model failure by incorporating the role of root-zone storage dynamics in the production of snowmelt runoff. Through transpiration, montane forests generate water storage deficits in the soils and weathered bedrock that comprise the root-zone. These deficits must be replenished by rain and snowmelt before significant runoff generation can occur. Overprediction of 2021 post-drought runoff in California can be primarily attributed to unprecedently large root-zone storage deficits.

1 Introduction

Mountain snowpack is an essential water reservoir for 1.9 billion people globally (Immerzeel et al., 2020). However, the accessibility of this water depends on how snowmelt runoff is generated. Historically, managers have relied on statistical relationships between snowpack and subsequent runoff for forecasting (DeWalle & Rango, 2008), but changes in climate can alter these relationships. Recently, in 2021 following a severe drought in California, streamflow forecasts by historically reliable multiple linear regression snowpack-runoff relationships (California Department of Water Resources, 2021) far exceeded actual streamflow (see for example, Figure 1a-b and site-specific versions of this figure in the Data Supplement). This led scientists and the public alike (Canon, 2021; Rogers, 2021) to wonder—where did the missing snowmelt go?

Previous work has proposed that shifts in streamflow generation from a given water input (snowpack) arise from differences in evapotranspiration (ET) due to changes in evaporative demand (Hamlet et al., 2007; Avanzi et al., 2020; Hoerling & Eischeid, 2007), snowmelt rate (Barnhart et al., 2016), and/or vegetation community (Boon, 2009; Pugh & Small, 2012; Knight et al., 1991). This effect may be particularly strong during multi-year droughts when ET can be a larger fraction of the annual water budget than usual (Massari et al., 2022). Antecedent moisture conditions have also been proposed to alter the relationship between water inputs and resulting streamflow (Hawkins & Ellis, 2010; Penna et al., 2011, 2015; Avanzi et al., 2020), including the role of rainfall inputs during the winter season and subsurface moisture conditions at the start of the winter season. Both of these factors can be tied to a form of runoff generation in which significant runoff occurs only after infiltrating water replenishes subsurface storage (McDonnell et al., 2021; Sayama et al., 2011). After the subsurface dries—typically through withdrawal of root-zone moisture by ET as shown in Figure 1d (Arkley, 1981; Bales et al., 2011; M. Anderson et al., 1995; Jones & Graham, 1993; Lewis & Burgy, 1964; Miller et al., 2010; Rose et al., 2003; Rempe & Dietrich, 2018; McCormick et al., 2021; Goulden

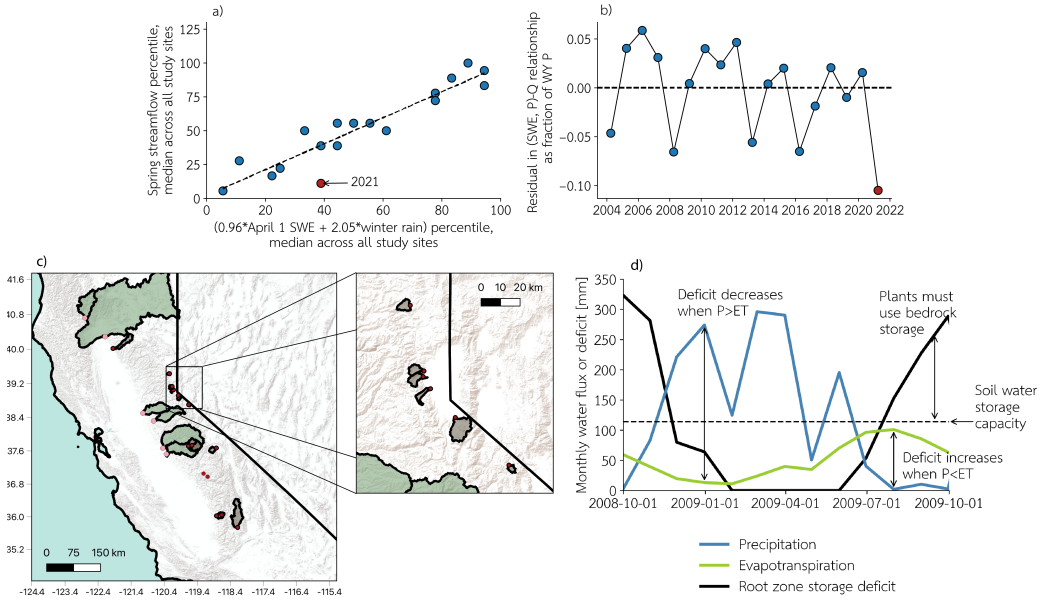

Figure 1. (a) Relationship between regression model for streamflow based on April 1 snow water equivalent (SWE) and winter rain and measured spring (April-July) streamflow summarized at 15 minimally disturbed sites for each year within the study period. This model is of a similar form to the one used by the California Department of Water Resources for streamflow forecasting. Points above the dashed line are years when the linear model underpredicts streamflow, and below the dashed line are years when the model overpredicts streamflow. SWE data is from SNODAS (National Operational Hydrologic Remote Sensing Center, 2000). (b) Median residual in the SWE-streamflow relationship among minimally disturbed sites as a fraction of April 1 SWE. (c) Map of study watersheds in the Sierra Nevada. Red dots mark gage locations for minimally disturbed sites shaded in grey, and pink dots for water supply basins shaded in green. (d) Explanatory plot for root-zone storage deficit. At the beginning of the wet season, the deficit decreases to 0 and remains there until ET exceeds P in the dry season. Deficit grows until the beginning of the next wet season. Deficits larger than soil water storage capacity indicate plant use of water stored in weathered bedrock.

& Bales, 2019; Klos et al., 2018; Hahm et al., 2020; Sayama et al., 2011)—infiltrating water goes first to replenishing this moisture deficit and then towards generating streamflow (McDonnell et al., 2021; Sayama et al., 2011). Less water input prior to snowmelt (i.e., winter rainfall) or more evapotranspiration during or prior to snowmelt (i.e., winter and spring ET) can limit how quickly the storage deficit is replenished—the precondition for significant streamflow generation. In this way, subsurface moisture conditions interact with above-ground factors to mediate runoff generation from snowpack.

Subsurface moisture deficits describe conditions in soils as well as the underlying weathered bedrock, which can account for a large portion of root-zone water storage (Bales et al., 2011; McCormick et al., 2021; K. J. Fowler et al., 2021; Ichii et al., 2009). Although there have been advances in large-scale observation of shallow soil moisture conditions (Entekhabi et al., 2010), deeper storage is less easy to monitor (Rempe & Dietrich, 2018) but still important for the water balance (McCormick et al., 2021). While storage changes recorded by the Gravity Recovery and Climate Experiment (GRACE) have been shown to be a strong predictor of subsequent streamflow (Sproles et al., 2015), GRACE data

are not finely resolved and include water storage effects (e.g., deep groundwater) that may not be relevant to the root-zone. Modeled subsurface water storage is, due to limited availability of deep water storage information, contingent on parameterization from available soil textural databases, which cannot account for storage dynamics in underlying bedrock (K. Fowler et al., 2020).

An alternative approach for estimating runoff-mediating subsurface moisture conditions is to track the balance between fluxes entering and exiting the root-zone. Spatially distributed, near real-time plant-driven water storage dynamics throughout both soil and bedrock can thus be quantified from precipitation and ET timeseries (Wang-Erlandsson et al., 2016; Dralle et al., 2021; Roche et al., 2020). Considering storage deficits in runoff prediction (Grindley, 1960) or as a harbinger of drought (Thomas et al., 2014; Geruo et al., 2017) is not new, but the widespread availability of distributed and increasingly reliable ET (Zhang et al., 2019), precipitation (Wang-Erlandsson et al., 2016), snow cover (as used by Dralle et al., 2021), and snow water equivalent (SWE) (Wrzesien et al., 2017) datasets now make it possible to monitor deficits in mountainous regions at large scales.

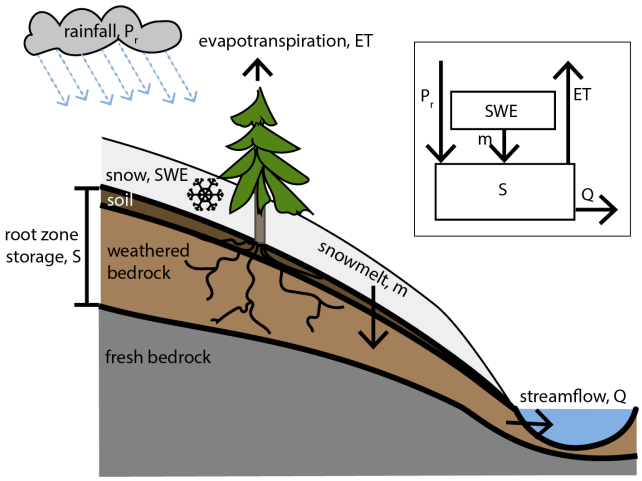

Figure 2. Conceptual hillslope diagram of mountain hydrology. Thin soils cover a deep, weathered bedrock zone that plants may access throughout the dry season. Snow accumulates during the winter and subsequently melts into the subsurface, while rain directly replenishes the subsurface. Evapotranspiration reduces water in storage, and streamflow is generated once a subsurface storage deficit is replenished. The inset diagram shows the two modeled water reservoirs (snow and root-zone storage) and fluxes (rainfall, snowmelt, evapotranspiration, and streamflow).

In this study, we introduce a mass-balance model for snowmelt driven runoff in a Mediterranean environment (wet winter, dry growing season) that explicitly incorporates the root-zone water storage deficit to explore the following hypothesized explanations for snowmelt runoff reduction (see Figure 2 for a schematic):

1. Less rainfall fell than normal during the spring;
2. Snowmelt rate was slower than normal;
3. Evaporative demand was higher than normal during the winter;
4. Evaporative demand was higher than normal during the spring;
5. The root-zone water storage deficit at the start of the wet season was larger than normal.

We validate our mass balance model against observed spring streamflow at 15 minimally disturbed sites in the Sierra Nevada and then develop a multiple linear regression model to quantify which drivers have the largest impact on snowmelt runoff. Based on results from the multiple linear regression analysis, we quantify improvement in snowmelt runoff forecasts in 2021 at 15 minimally disturbed watersheds as well as 6 watersheds important for California's water supply. While we specifically explore the fate of the 'missing' 2021 snowmelt runoff in California, our goal is to understand how subsurface water storage dynamics—in combination with other previously studied mechanisms—inform forecasting of snowmelt runoff in general.

2 Methods

2.1 Mass-balance snowmelt runoff model

Here we expand upon a stochastic hydrological model (Hahm et al., 2019) that incorporates storage as a simple 1-d bucket to describe annual runoff dynamics and plant water availability in Mediterranean catchments. In the original model, precipitation P [L] contributes water to storage during the wet season, and evapotranspiration ET [L] removes water from storage primarily during the dry season. Streamflow is generated only if the subsurface storage reservoir is full. The root-zone is treated as a single storage reservoir representing a thin soil layer underlain by deep weathered bedrock (Figure 2), as is common in forested mountainous environments (Holbrook et al., 2014; McCormick et al., 2021; Wald et al., 2013; Amundson et al., 2015). The model does not specify where water is stored within the root-zone or its energy state (e.g., saturated versus unsaturated). Nor does it mechanistically specify how groundwater produces streamflow at the hillslope-channel boundary, only that water input volumes in excess of the deficit generate flow in the stream.

In our model formulation, storage dynamics evolve annually over three hydrological seasons: a winter wet season when rain enters storage and snow accumulates, a snowmelt season when rain and snowmelt enter storage, and a dry summer season. ET draws from storage at different rates in each season. Starting at the beginning of the wet season, there is a deficit generated by the previous dry season that shrinks with water input during the winter wet season and snowmelt periods (Figure 1d). Once the deficit is reduced to 0, streamflow is generated. When ET exceeds snowmelt and rain in the spring, streamflow stops, and the deficit grows again until the start of the next wet season. Snowmelt runoff emerges as the net water input during the melt season (snowmelt and precipitation less ET) once the deficit has been met. This mass balance results in an expression for spring streamflow (Q [L], normalized by catchment area), in which each of the proposed factors that could impact the relationship between snowpack and streamflow appear as variables:

$$Q = \begin{cases} \text{if } P_w - ET_w > D_{Oct1}: \\ \quad \max(0, SWE - ET_{net} N_{melt}) \\ \text{otherwise:} \\ \quad \max(0, SWE - ET_{net} N_{melt} - \\ \qquad\qquad D_{Oct1} + (P_w - ET_w)) \end{cases} \tag{1}$$

where P_w [L] is winter rainfall, ET_w [L] is winter ET, D_{Oct1} [L] is the deficit at the beginning of the wet season, SWE [L] is April 1 snowpack, $ET_{net} = ET_s - P_s$ [L/T] is the mean spring ET rate ET_s less the mean spring precipitation rate P_s, and N_{melt} [T] the length of the snowmelt period. A table of notation is in Supplementary Table S2. In Figure 2, $P_r = P_w + P_s$. Both conditions are bounded by zero since streamflow cannot be negative. A negative value for either condition indicates that water demand from ET exceeds water availability from rain and snowmelt, so streamflow must be zero. In Equation 1, all of the hypotheses listed at the end of the introduction for missing snowmelt

appear: (1) rain appears in P_w and P_s, (2) snowmelt rate appears in $N_{melt} = SWE/m$, (3) ET appears in ET_s and ET_w, and (4) the deficit appears as D_{Oct1}. For a full description of the model, see Supplemental Information S2.

2.2 A regression model for snowmelt-driven runoff

We performed exploratory data analysis to determine which hypotheses listed at the end of the introduction best explain snowmelt runoff at the study sites (Figure 1c). See Supplemental Information S1 for details on study sites and site selection criteria, and Supplemental Information S6 for additional details on exploratory analysis. To determine which mechanisms have the most explanatory power for deviations from the snowpack-runoff relationship, we developed a multiple linear regression equation at each study site:

$$Q = C_1\ SWE + C_2 P_w + C_3 \frac{D_{Oct1}}{P} + C_4 \frac{ET_{net} N_{melt}}{P} + C_5 \frac{ET_w - P_w}{P} + C_6 \frac{m}{ET_{net}} + C_7, \quad (2)$$

where $C_1, ..., C_7$ are fitted parameters.

Each variable other than SWE, m/ET_{net} and P_w is expressed as a fraction of water year precipitation. Expressing variables relative to water year P strengthens the relationship between variables and residuals in the SWE-Q relationship. This normalization also has the effect of minimizing correlation between variables since many model variables are correlated with water year P. In Equation 2, $ET_{net}N_{melt}/P$ and $(ET_w - P_w)/P$ capture effects of variable ET (Hypotheses 3 and 4 in the conceptual runoff model section), $(ET_{net}N_{melt})/P$ captures effects of variable spring rainfall (Hypothesis 1), m/ET_{net} captures effects of variable snowmelt rate (Hypothesis 2), and D_{Oct1}/P captures effects of variable root-zone storage deficit (Hypothesis 4). Since the relationships among the study variable may not be linear, we also used a random forest model to corroborate the findings of this regression approach; see Supplemental Information S7 for additional details.

2.3 Data sources and data processing

Details on site selection criteria for the 15 minimally disturbed basins and site characteristics for all study basins are found in Supplemental Information S1.

Streamflow data for all sites other than P300 and B200 were obtained from the National Water Information System (NWIS) (U.S. Geological Survey, 2021) using the package hydrofunctions (`https://hydrofunctions.readthedocs.io/en/master/`). Streamflow data from P300 and B200 were obtained from the Kings River Experimental watersheds of the US Forest Service Pacific Southwest Research Station (Hunsaker & Safeeq, 2017) for years 2006-2015, and data for 2015-2021 were collected and processed in the same manner as the published 2006-2015 data. Daily snow water equivalent was obtained using Snow Data Assimilation System (SNODAS) (National Operational Hydrologic Remote Sensing Center, 2000). Precipitation data were obtained from Parameter-elevation Regressions on Independent Slopes Model (PRISM) (PRISM Climate Group, 2004). Evapotranspiration and temperature data were obtained from PML V2 (Zhang et al., 2019; Gan et al., 2018; Zhang et al., 2016) and Moderate Resolution Imaging Spectroradiometer (MODIS) (Running et al., 2017). PRISM, MODIS, and PML V2 were accessed via the Google Earth Engine Python API (Gorelick et al., 2017). Evaporative stress index (ESI) data were obtained from ClimateServ (M. Anderson et al., 1997; M. C. Anderson et al., 2007a, 2007b, 2011). ESI provides a measure of ET anomalies over time using thermal satellite imagery. A higher ESI indicates a larger positive ET anomaly, whereas lower or negative values indicate depressed ET. For comparison with root-zone storage deficit,

we included soil water storage capacity (Soil Survey Staff, 2019) as processed by McCormick et al. (2021).

For the majority of the study period, we use the PML V2 data set for ET. This data set, when combined with PRISM, results in calculated subsurface storage deficits consistent with field measurements (McCormick et al., 2021). Since PML V2 is not yet available through the 2021 water year, we extended the PML V2 data set using MODIS ET. We bias-corrected MODIS ET to PML V2 using a basin-specific linear relationship for each study watershed. For most watersheds, the correlation between PML V2 and MODIS ET is strong (median R^2 >0.4, see Supplementary Code (Lapides et al., 2021b)).

Snowmelt rate was calculated from daily SNODAS data as in Barnhart et al. (2016):

$$m = \frac{\Sigma|min(\Delta SWE_t, 0)|}{\Sigma\Delta_t}, \tag{3}$$

where the numerator is the sum of all daily differences in SWE on days when SWE decreases, and Δ_t is 1 on days when SWE decreases and otherwise 0. See Supplemental Information S3 for a description of concordance checks between SNODAS and PRISM.

The root-zone storage deficit was calculated following Wang-Erlandsson et al. (2016) and Dralle et al. (2021). The only difference here is that instead of using only precipitation and evapotranspiration (Wang-Erlandsson et al., 2016) or approximating information about snow using snow cover (Dralle et al., 2021), we used SNODAS data directly to represent accumulation and melt of snowpack. For a full description of deficit calculations, see Supplemental Information S4. For a justification of why this deficit is specifically a 'root-zone' storage deficit, refer to Supplemental Information S9.

3 Results

The mass balance model of root-zone storage (Equation 1) accurately predicts measured spring streamflow (NSE=0.79, see Figure 3a) at 15 minimally disturbed sites in the Sierra Nevada (grey sites in Figure 1c). Panels b-e plot these same predictions, showing scatter points colored by actual spring streamflow against heatmaps generated from the mass balance model. Good model performance despite a lack of tunable parameters suggests that the model captures the primary mechanisms for spring streamflow generation at the study sites.

3.1 Root-zone storage deficit is important for determining runoff from snowpack

We regressed spring runoff (April-July, proxy for snowmelt runoff) on the variables identified in the storage-based modeling framework (Equation 2) at the 15 minimally disturbed sites to quantitatively rank the importance of different physical drivers of snowmelt runoff generation during years following both wet (above 75th percentile of annual precipitation) and dry (below 25th percentile of annual precipitation) years (Figure 4a). Model outcomes in both wet and dry years are most sensitive to snowpack and winter rainfall, the two parameters included in the forecasting model used as an example in this study. Assuming first-order effects are captured by the model, the remaining variables (shown in Figure 4a) must explain performance failure in 2021. Of these four variables, only the effect size of the deficit is larger in years following dry years than wet years, and it is substantially larger, making it by far the most important term in years following dry years, even larger than winter rainfall (not shown). This suggests that large deficits generated during dry years play an essential role in reducing snowmelt runoff in the following year. See Supplemental Tables S5 and S6 for effect sizes for all variables at all sites on wet and dry years.

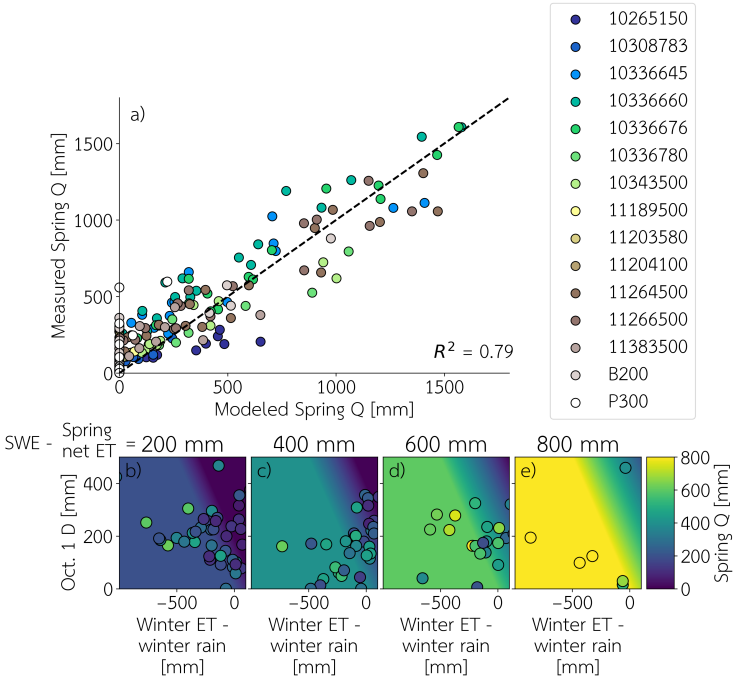

Figure 3. (a) Comparison between measured spring streamflow at minimally disturbed study sites and predicted streamflow based on Equation 1. Legend refers to USGS streamgauge ID or USFS ID number for B200 and P300. (b-e) Heatmaps showing how modeled streamflow varies based on each model parameter. Within each panel: winter ET - winter rain increases moving right, and October 1 deficit increases vertically. Moving to the right between panels, April 1 SWE - (spring ET - spring rain) increases. Points plotted on heatmaps represent a single water year for a study site and are colored by measured spring streamflow. Points are plotted on the heatmaps if $SWE - ET_{net}N_{melt}$ is within 100 mm of the value labeled for each panel.

With rare exceptions, the sign for each effect size matches the expected sign based on hypothesized model mechanisms at all sites (see Supplemental Tables S5 and S6), providing further evidence for the proposed conceptual framework. No more than one site shows an unexpected sign for any parameter except for the melt rate, which has an unexpected sign at 4 sites, and (surprisingly) winter rain, which has an unexpected sign at 3 sites. Given the melt rate's small effect sizes and unexpected effect signs, we conclude that melt rate is relatively insignificant in comparison to other explanatory variables. The same conclusion cannot be drawn for winter rain because its effect size is very large. Instead, we suggest that at those sites with an unexpected sign for winter rainfall there may be either (1) a negative relationship between total precipitation or SWE and winter rainfall during the study period that confounds interpretation of the winter rainfall coefficient or (2) errors in precipitation from PRISM due to the small size of the catchments. The median Nash-Sutcliffe Efficiency (NSE) value for multiple linear regression models across the study sites is 0.92.

We also trained a single random forest model to predict spring streamflow at all sites based on the same set of input parameters (model performance NSE=0.98) since a linear model may not account for complex interactions between the hydrologic processes used in the regression. Results from the random forest analysis also support the hypothesized mechanisms; contribution of parameters to model outputs as measured by feature importance confirms that October 1 deficit and spring net ET are important drivers of

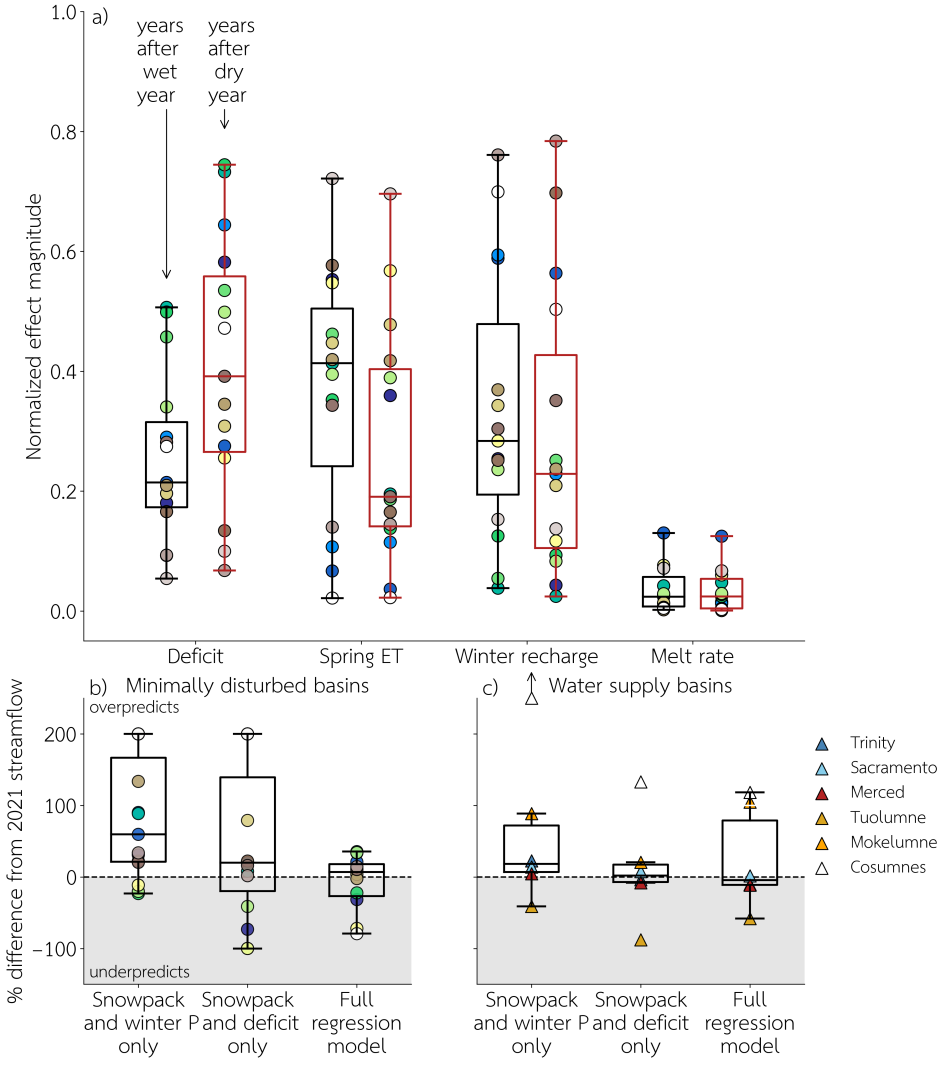

Figure 4. (a) Normalized effect magnitude of each variable included in the multiple linear regression for snowmelt runoff at all sites, comparing the set of years following wet years to years following dry years. Snowpack and winter rainfall (excluded from plot) are consistently the most important variables. Variable names are described for the water balance feature they represent, but deficit, spring net ET, and winter recharge are relative to water year precipitation, and melt rate is relative to spring net ET. Box and whisker plot shows median value across all minimally disturbed sites. Effect size is the coefficient for a given variable multiplied by the median absolute value of the variable for years following wet (black) or dry (red) years. Normalization is achieved by scaling effect sizes for each site so that absolute values sum to 1. Performance of regression models in 2021 at (b) 15 minimally disturbed and (c) 6 water supply basins. Legend for panels a) and b) is the same as for Figure 3a.

snowmelt runoff, whereas the melt rate is less important. See Supplemental Information S7 for more details.

3.2 Using deficits increases predictive power of forecasting models following drought

A linear regression model using snowpack and winter rainfall (Figure 1a) replicates the 2021 "missing" streamflow phenomenon with a similar magnitude of error in 2021 (California Department of Water Resources, 2021). Linear regressions of this type have been used by the California Department of Water Resources (personal communication with Sean de Guzman, chief of the California Department of Water Resources Snow Surveys and Water Supply Forecasting Section) and in research applications exploring snowpack-runoff relationships (Godsey et al., 2014). By including a term representing the deficit (linear regression using only snowpack and deficit) rather than winter rainfall, model performance on years following dry years improves from a median of NSE=0.42 to a median NSE of 0.62. For site-specific details, see Supplemental Table S7.

When focusing on the 2021 water year, gains in forecast skill are striking. Figure 4b shows predictions for 2021 streamflow at the minimally disturbed sites using the full multiple linear regression model, snowpack and deficit only, and snowpack and winter rain only. Each regression model is trained on data from the full study period. Using only snowpack and rainfall, the model over-predicts the 2021 streamflow at all minimally disturbed sites by a median of 60%. Using the full regression model, median streamflow is only over-predicted by 7%, and with snowpack and deficit it is over-predicted by only 20%.

We tested our model on minimally disturbed basins. However, given that the deficit is calculated using remotely-sensed evapotranspiration, it should be sensitive to spatial variation in land-cover or forms of disturbance, such as fire, that are known to impact patterns of plant water use (Lowman & Barros, 2019; Boisramé et al., 2017; Pausas & Keeley, 2019; Renninger et al., 2013). This suggests our model may be applicable to larger and more complex basins. We therefore also applied the model to six watersheds central to California's water supply (green basins in Figure 1c and Supplemental Information S1 for additional site information). As shown in Figure 4c, adding a term to a linear regression model to represent the deficit improves error in prediction of 2021 streamflow from a median of 18% to 2% overprediction. With the full regression, streamflow is underpredicted by a median of 4%. The sum of errors across the water supply basins is reduced from 34% to 3% with the inclusion of the deficit. Therefore, despite noise introduced by fire and logging legacies, incorporating the root-zone storage deficit into models for spring streamflow from snowpack substantially improves model performance for water resources-relevant forecasting, especially following dry years.

4 Discussion and conclusions

Large drought-induced root-zone storage deficits at the start of the 2021 wet season led to the "missing" streamflow phenomenon. Adding a term to describe root-zone storage deficit decreased total overprediction of 2021 snowmelt runoff in a linear regression model from a 60% to 20% across minimally disturbed study basins and 18% to 2% across water supply basins, an essential improvement for water resources management. Not only does October 1 deficit drive reductions in streamflow following dry years, but it can be quantified prior to the snowmelt season for the purpose of improved snowmelt runoff forecasting.

Managers and researchers have long recognized the importance of subsurface moisture conditions for subsequent runoff (Arkley, 1981; Bales et al., 2011; M. Anderson et al., 1995; Jones & Graham, 1993; Lewis & Burgy, 1964; Miller et al., 2010; Rose et al., 2003; Rempe & Dietrich, 2018; McCormick et al., 2021; Goulden & Bales, 2019; Klos et al., 2018; Hahm et al., 2021; Sayama et al., 2011; Grindley, 1960); however, incorporating root-zone water storage dynamics into forecasting presents a challenge. This is due

to both the limited available data on water storage in weathered bedrock, as well as the challenge of understanding interactions between different drivers of root-zone dynamics. The presented model quantitatively captures the expected importance of subsurface moisture conditions for runoff forecasting, providing a low-complexity solution to the problem of runoff prediction, without reliance on water storage parameters that are poorly constrained at large spatial scales (Wang-Erlandsson et al., 2016; Dralle et al., 2021). The model captures snowmelt runoff well following dry years, which is essential given the projected increase in "weather whiplash", i.e., alternation between extreme wet and dry years (Persad et al., 2020).

While simple, the good performance of our mass-balance model suggests that first-order hydrological behavior is captured. A more complex model may capture additional site-specific nuance, but a simple model provides high-level insight into the drivers of changes in hydrological function. A further implication of good performance of our mass balance model is that runoff generation in the Sierra is not highly dependent on infiltration-excess overland flow processes, which is not included as a runoff process in our model and should be relatively insensitive to root-zone storage deficits (Castillo et al., 2003). Instead, the agreement between the presented model and data supports the hypothesis that replenishment of root-zone storage deficits is required for significant runoff generation to occur, which is more consistent with saturation overland (Dunne & Black, 1970) or subsurface (Freeze, 1972) flow generation mechanisms. Additionally, since the data used in this study are gridded, the spatial distribution of precipitation and evapotransiration are neglected. Thus, the good performance of our model also suggests that heterogeneity in these fluxes may not be of first-order importance for spring streamflow generation at the study sites.

Climate change is impacting the reliability and predictability of water supply in many ways, one of which is post-drought reductions in expected snowmelt runoff. Root-zone storage deficits provide a means of monitoring changing conditions, but operationalizing deficits in real-time requires the development of frequently-updated, reliable, large-scale evapotranspiration and precipitation datasets. Multiple data products are being developed and tested in the community to support urgent needs for research and management applications (Guo et al., 2022; Mazzoleni et al., 2019), and the present study provides yet more motivation to continue honing these essential datasets.

5 Open Research

Data and code generated for this publication are available in an online data repository, `https://github.com/lapidesd/CA_missing_freshet`, (Lapides et al., 2021b). Raster maps of percentiles of April 1 SWE are available at `https://www.hydroshare.org/resource/4b940b8593a4416e954a47bbbc58c568/` (Lapides et al., 2021a). Primary analyses are available as Google Colab notebooks: (i) exploration of relationship between April 1 SWE and spring runoff at each study site (`https://colab.research.google.com/drive/1tv8kbIe9EY3vFdAQzbJTfE7?usp=sharing`), (ii) calculation of all quantities used in analysis and exploring the four hypotheses stated at the end of the introduction (`https://colab.research.google.com/drive/1hq-qqlIR_LuEyZ5s5RPddnqDLBo4M309?usp=sharing`), (iii) development of a random forest model and a multiple linear regression model for spring streamflow and examines the results (`https://colab.research.google.com/drive/1jPtdcESsGPfB2H6MC-W7metpiFSqe799?usp=sharing`), (iv) implementation of the mass-balance model (`https://colab.research.google.com/drive/197Hglpe3kkThdblSFz-9U9h63IvdQzE9?usp=sharing`, and (v) exploring predictive improvement by adding the deficit at 6 economically important watersheds in California (`https://colab.research.google.com/drive/1qVGwArARfvwO_dLbAqZdhGnEUV_TB6gP?usp=sharing`).

Acknowledgments

We would like to thank Sean de Guzman, chief of the California Department of Water Resources Snow Surveys and Water Supply Forecasting Section, for providing insight into how runoff is forecast in California. Funding was provided by Simon Fraser University, a Natural Sciences and Engineering Research Council of Canada Discovery Grant, and the USDA Forest Service Pacific Southwest Research Station with funds administered by Oak Ridge Institute for Science and Education (ORISE).

References

Amundson, R., Heimsath, A., Owen, J., Yoo, K., & Dietrich, W. E. (2015). Hillslope soils and vegetation. *Geomorphology*, *234*, 122–132.

Anderson, M., Graham, R., Alyanakian, G., & Martynn, D. (1995). Late summer water status of soils and weathered bedrock in a giant sequoia grove. *Soil Science*, *160*(6), 415–422.

Anderson, M., Norman, J., Diak, G., Kustas, W., & Mecikalski, J. (1997). A two-source time-integrated model for estimating surface fluxes using thermal infrared remote sensing. *Remote sensing of environment*, *60*(2), 195–216.

Anderson, M. C., Hain, C., Wardlow, B., Pimstein, A., Mecikalski, J. R., & Kustas, W. P. (2011). Evaluation of drought indices based on thermal remote sensing of evapotranspiration over the continental united states. *Journal of Climate*, *24*(8), 2025–2044.

Anderson, M. C., Norman, J. M., Mecikalski, J. R., Otkin, J. A., & Kustas, W. P. (2007a). A climatological study of evapotranspiration and moisture stress across the continental united states based on thermal remote sensing: 1. model formulation. *Journal of Geophysical Research: Atmospheres*, *112*(D10).

Anderson, M. C., Norman, J. M., Mecikalski, J. R., Otkin, J. A., & Kustas, W. P. (2007b). A climatological study of evapotranspiration and moisture stress across the continental united states based on thermal remote sensing: 2. surface moisture climatology. *Journal of Geophysical Research: Atmospheres*, *112*(D11).

Arkley, R. J. (1981). Soil moisture use by mixed conifer forest in a summer-dry climate. *Soil Science Society of America Journal*, *45*(2), 423–427.

Avanzi, F., Rungee, J., Maurer, T., Bales, R., Ma, Q., Glaser, S., & Conklin, M. (2020). Climate elasticity of evapotranspiration shifts the water balance of mediterranean climates during multi-year droughts. *Hydrology and Earth System Sciences*, *24*(9), 4317–4337.

Bales, R. C., Hopmans, J. W., O'Geen, A. T., Meadows, M., Hartsough, P. C., Kirchner, P., ... Beaudette, D. (2011). Soil moisture response to snowmelt and rainfall in a sierra nevada mixed-conifer forest. *Vadose Zone Journal*, *10*(3), 786–799.

Barnhart, T. B., Molotch, N. P., Livneh, B., Harpold, A. A., Knowles, J. F., & Schneider, D. (2016). Snowmelt rate dictates streamflow. *Geophysical Research Letters*, *43*(15), 8006–8016.

Boisramé, G., Thompson, S., Collins, B., & Stephens, S. (2017). Managed wildfire effects on forest resilience and water in the sierra nevada. *Ecosystems*, *20*(4), 717–732.

Boon, S. (2009). Snow ablation energy balance in a dead forest stand. *Hydrological Processes: An International Journal*, *23*(18), 2600–2610.

California Department of Water Resources. (2021). *Dwr bulletin-120 forecast performance, water year 2021.* (accessed at `https://tableau.cnra.ca.gov/t/DWR\_Snow\_WSFcast/views/WY2021Performance/Dashboard1?\%3Adisplay\_count=n\&\%3Aembed=y\&\%3AisGuestRedirectFromVizportal=y\&\%3Aorigin=viz\_share\_link\&\%3AshowAppBanner=false\&\%3AshowVizHome=n`)

Canon, G. (2021). 'truly an emergency': how drought returned to california – and what lies ahead. *Guardian*. (accessed at `https://www.theguardian.com/us-news/2021/jun/07/california-drought-oregon-west-climate-change`)

Castillo, V., Gomez-Plaza, A., & Martınez-Mena, M. (2003). The role of antecedent soil water content in the runoff response of semiarid catchments: a simulation approach. *Journal of Hydrology*, *284*(1-4), 114–130.

DeWalle, D. R., & Rango, A. (2008). *Principles of snow hydrology*. Cambridge University Press.

Dralle, D. N., Hahm, W. J., Chadwick, K. D., McCormick, E., & Rempe, D. M. (2021). Accounting for snow in the estimation of root zone water storage capacity from precipitation and evapotranspiration fluxes. *Hydrology and Earth System Sciences*, *25*(5), 2861–2867.

Dunne, T., & Black, R. D. (1970). An experimental investigation of runoff production in permeable soils. *Water Resources Research*, *6*(2), 478–490.

Entekhabi, D., Njoku, E. G., O'Neill, P. E., Kellogg, K. H., Crow, W. T., Edelstein, W. N., ... others (2010). The soil moisture active passive (smap) mission. *Proceedings of the IEEE*, *98*(5), 704–716.

Fowler, K., Knoben, W., Peel, M., Peterson, T., Ryu, D., Saft, M., ... Western, A. (2020). Many commonly used rainfall-runoff models lack long, slow dynamics: Implications for runoff projections. *Water Resources Research*, *56*(5), e2019WR025286.

Fowler, K. J., Coxon, G., Freer, J. E., Knoben, W. J., Peel, M. C., Wagener, T., ... Zhang, L. (2021). Towards more realistic runoff projections by removing limits on simulated soil moisture deficit. *Journal of Hydrology*, *600*, 126505.

Freeze, R. A. (1972). Role of subsurface flow in generating surface runoff: 1. base flow contributions to channel flow. *Water Resources Research*, *8*(3), 609–623.

Gan, R., Zhang, Y., Shi, H., Yang, Y., Eamus, D., Cheng, L., ... Yu, Q. (2018). Use of satellite leaf area index estimating evapotranspiration and gross assimilation for australian ecosystems. *Ecohydrology*, *11*(5), e1974.

Geruo, A., Velicogna, I., Kimball, J. S., Du, J., Kim, Y., Colliander, A., & Njoku, E. (2017). Satellite-observed changes in vegetation sensitivities to surface soil moisture and total water storage variations since the 2011 texas drought. *Environmental Research Letters*, *12*(5), 054006.

Godsey, S. E., Kirchner, J. W., & Tague, C. L. (2014). Effects of changes in winter snowpacks on summer low flows: case studies in the sierra nevada, california, usa. *Hydrological Processes*, *28*(19), 5048–5064.

Gorelick, N., Hancher, M., Dixon, M., Ilyushchenko, S., Thau, D., & Moore, R. (2017). Google earth engine: Planetary-scale geospatial analysis for everyone. *Remote sensing of Environment*, *202*, 18–27.

Goulden, M. L., & Bales, R. C. (2019). California forest die-off linked to multi-year deep soil drying in 2012–2015 drought. *Nature Geoscience*, *12*(8), 632–637.

Grindley, J. (1960). Calculated soil moisture deficits in the dry summer of 1959 and forecast dates of first appreciable runoff. *Int. Ass. Sci. HydroL*, 109–20.

Guo, X., Wu, Z., He, H., & Xu, Z. (2022). Evaluating the potential of different evapotranspiration datasets for distributed hydrological model calibration. *Remote Sensing*, *14*(3), 629.

Hahm, W. J., Dralle, D., Rempe, D., Bryk, A., Thompson, S., Dawson, T., & Dietrich, W. (2019). Low subsurface water storage capacity relative to annual rainfall decouples mediterranean plant productivity and water use from rainfall variability. *Geophysical Research Letters*, *46*(12), 6544–6553.

Hahm, W. J., Dralle, D. N., Sanders, M., Bryk, A. B., Fauria, K. E., Huang, M.-H., ... others (2021). Bedrock vadose zone storage dynamics under extreme drought: consequences for plant water availability, recharge, and runoff. *ESSOAR Pre-Print (https://www.essoar.org/doi/abs/10.1002/essoar.10509661.2)*.

Hahm, W. J., Rempe, D., Dralle, D., Dawson, T., & Dietrich, W. (2020). Oak transpiration drawn from the weathered bedrock vadose zone in the summer dry season. *Water Resources Research. 56 (11): e2020WR027419*, *56*(11).

Hamlet, A. F., Mote, P. W., Clark, M. P., & Lettenmaier, D. P. (2007). Twentieth-century trends in runoff, evapotranspiration, and soil moisture in the western united states. *Journal of Climate*, *20*(8), 1468–1486.

Hawkins, T., & Ellis, A. (2010). The dependence of streamflow on antecedent subsurface moisture in an arid climate. *Journal of arid environments*, *74*(1), 75–86.

Hoerling, M., & Eischeid, J. (2007). Past peak water in the southwest. *Southwest Hydrology*, *6*(1), 18–19.

Holbrook, W. S., Riebe, C. S., Elwaseif, M., L. Hayes, J., Basler-Reeder, K., L. Harry, D., ... W. Hopmans, J. (2014). Geophysical constraints on deep weathering and water storage potential in the southern sierra critical zone observatory. *Earth Surface Processes and Landforms*, *39*(3), 366–380.

Hunsaker, C. T., & Safeeq, M. (2017). Kings river experimental watersheds stream discharge.
doi: 10.2737/RDS-2017-0037

Ichii, K., Wang, W., Hashimoto, H., Yang, F., Votava, P., Michaelis, A. R., & Nemani, R. R. (2009). Refinement of rooting depths using satellite-based evapotranspiration seasonality for ecosystem modeling in california. *Agricultural and Forest Meteorology*, *149*(11), 1907–1918.

Immerzeel, W. W., Lutz, A., Andrade, M., Bahl, A., Biemans, H., Bolch, T., ... others (2020). Importance and vulnerability of the world's water towers. *Nature*, *577*(7790), 364–369.

Jones, D., & Graham, R. (1993). Water-holding characteristics of weathered granitic rock in chaparral and forest ecosystems. *Soil Science Society of America Journal*, *57*(1), 256–261.

Klos, P. Z., Goulden, M. L., Riebe, C. S., Tague, C. L., O'Geen, A. T., Flinchum, B. A., ... others (2018). Subsurface plant-accessible water in mountain ecosystems with a mediterranean climate. *Wiley Interdisciplinary Reviews: Water*, *5*(3), e1277.

Knight, D. H., Yavitt, J. B., & Joyce, G. D. (1991). Water and nitrogen outflow from lodgepole pine forest after two levels of tree mortality. *Forest Ecology and Management*, *46*(3-4), 215–225.

Lapides, D. A., Hahm, W. J., Rempe, D. M., & Dralle, D. N. (2021a). *April 1 swe spatial percentiles using snodas for the contiguous usa.* (accessed at `https://www.hydroshare.org/resource/4b940b8593a4416e954a47bbbc58c568/`)

Lapides, D. A., Hahm, W. J., Rempe, D. M., & Dralle, D. N. (2021b). *Supplementary code and data for: Root zone storage deficits mediate the production of streamflow from snowmelt.* (accessed at `https://github.com/lapidesd/CA\_missing\_freshet`) doi: 10.5281/zenodo.6144807

Lewis, D., & Burgy, R. H. (1964). The relationship between oak tree roots and groundwater in fractured rock as determined by tritium tracing. *Journal of Geophysical Research*, *69*(12), 2579–2588.

Lowman, L., & Barros, A. P. (2019). Fire-induced canopy changes alter plant water, energy and carbon relations for coastal plains forests in the southeast us. In *Agu fall meeting abstracts* (Vol. 2019, pp. B53H–2500).

Massari, C., Avanzi, F., Bruno, G., Gabellani, S., Penna, D., & Camici, S. (2022). Evaporation enhancement drives the european water-budget deficit during multi-year droughts. *Hydrology and Earth System Sciences*, *26*(6), 1527–1543.

Mazzoleni, M., Brandimarte, L., & Amaranto, A. (2019). Evaluating precipitation datasets for large-scale distributed hydrological modelling. *Journal of Hydrology*, *578*, 124076.

McCormick, E. L., Dralle, D. N., Hahm, W. J., Tune, A. K., Schmidt, L. M., Chadwick, K. D., & Rempe, D. M. (2021). Widespread woody plant use of water stored in bedrock. *Nature*, *597*(7875), 225–229.

McDonnell, J. J., Spence, C., Karran, D. J., Ilja van Meerveld, H., & Harman, C. (2021). Fill-and-spill: A process description of runoff generation at the scale of the beholder. *Water Resources Research*, e2020WR027514.

Miller, G. R., Chen, X., Rubin, Y., Ma, S., & Baldocchi, D. D. (2010). Groundwater uptake by woody vegetation in a semiarid oak savanna. *Water Resources Research*, *46*(10).

National Operational Hydrologic Remote Sensing Center. (2000). *Snow data assimilation system (snodas) data products at nsidc, version 1.* Boulder, Colorado USA. NSIDC: National Snow and Ice Data Center. doi: \url{https://doi.org/10.7265/N5TB14TC}

Pausas, J. G., & Keeley, J. E. (2019). Wildfires as an ecosystem service. *Frontiers in Ecology and the Environment*, *17*(5), 289–295.

Penna, D., Tromp-van Meerveld, H., Gobbi, A., Borga, M., & Dalla Fontana, G. (2011). The influence of soil moisture on threshold runoff generation processes in an alpine headwater catchment. *Hydrology and Earth System Sciences*, *15*(3), 689–702.

Penna, D., van Meerveld, H. J., Oliviero, O., Zuecco, G., Assendelft, R., Dalla Fontana, G., & Borga, M. (2015). Seasonal changes in runoff generation in a small forested mountain catchment. *Hydrological Processes*, *29*(8), 2027–2042.

Persad, G. G., Swain, D. L., Kouba, C., & Ortiz-Partida, J. P. (2020). Inter-model agreement on projected shifts in california hydroclimate characteristics critical to water management. *Climatic Change*, *162*(3), 1493–1513.

PRISM Climate Group. (2004). *Prism rainfall dataset.* (accessed at `http://prism.oregonstate.edu`)

Pugh, E., & Small, E. (2012). The impact of pine beetle infestation on snow accumulation and melt in the headwaters of the colorado river. *Ecohydrology*, *5*(4), 467–477.

Rempe, D. M., & Dietrich, W. E. (2018). Direct observations of rock moisture, a hidden component of the hydrologic cycle. *Proceedings of the National Academy of Sciences*, *115*(11), 2664–2669.

Renninger, H. J., Clark, K. L., Skowronski, N., & Schäfer, K. V. (2013). Effects of a prescribed fire on water use and photosynthetic capacity of pitch pines. *Trees*, *27*(4), 1115–1127.

Roche, J. W., Ma, Q., Rungee, J., & Bales, R. C. (2020). Evapotranspiration mapping for forest management in california's sierra nevada. *Frontiers in Forests and Global Change*, *3*, 69.

Rogers, P. (2021). Where did sierra snow go this spring? not into California rivers and water supplies. *The Mercury News*.

Rose, K., Graham, R., & Parker, D. (2003). Water source utilization by pinus jeffreyi and arctostaphylos patula on thin soils over bedrock. *Oecologia*, *134*(1), 46–54.

Running, S., Mu, Q., & Zhao, M. (2017). *Mod16a2 modis/terra net evapotranspiration 8-day l4 global 500m sin grid v006 [data set]. nasa eosdis land processes daac.* doi: \url{https://doi.org/10.5067/MODIS/MOD16A2.006}

Sayama, T., McDonnell, J. J., Dhakal, A., & Sullivan, K. (2011). How much water can a watershed store? *Hydrological Processes*, *25*(25), 3899–3908.

Soil Survey Staff. (2019). *Gridded national soil survey geographic (gnatsgo) database for the conterminous united states.* USDA. (`https://nrcs.app.box.com/v/soils`)

Sproles, E., Leibowitz, S., Reager, J., Wigington Jr, P., Famiglietti, J., & Patil, S. (2015). Grace storage-runoff hystereses reveal the dynamics of regional

watersheds. *Hydrology and Earth System Sciences*, *19*(7), 3253–3272.

Thomas, A. C., Reager, J. T., Famiglietti, J. S., & Rodell, M. (2014). A grace-based water storage deficit approach for hydrological drought characterization. *Geophysical Research Letters*, *41*(5), 1537–1545.

U.S. Geological Survey. (2021). *National water information system data available on the world wide web (water data for the nation).* (accessed December 2021)

Wald, J. A., Graham, R. C., & Schoeneberger, P. J. (2013). Distribution and properties of soft weathered bedrock at $\leq$1 m depth in the contiguous united states. *Earth Surface Processes and Landforms*, *38*(6), 614–626.

Wang-Erlandsson, L., Bastiaanssen, W. G., Gao, H., Jägermeyr, J., Senay, G. B., Van Dijk, A. I., ... Savenije, H. H. (2016). Global root zone storage capacity from satellite-based evaporation. *Hydrology and Earth System Sciences*, *20*(4), 1459–1481.

Wrzesien, M. L., Durand, M. T., Pavelsky, T. M., Howat, I. M., Margulis, S. A., & Huning, L. S. (2017). Comparison of methods to estimate snow water equivalent at the mountain range scale: A case study of the california sierra nevada. *Journal of Hydrometeorology*, *18*(4), 1101–1119.

Zhang, Y., Kong, D., Gan, R., Chiew, F. H., McVicar, T. R., Zhang, Q., & Yang, Y. (2019). Coupled estimation of 500 m and 8-day resolution global evapotranspiration and gross primary production in 2002–2017. *Remote Sensing of Environment*, *222*, 165–182.

Zhang, Y., Peña-Arancibia, J. L., McVicar, T. R., Chiew, F. H., Vaze, J., Liu, C., ... others (2016). Multi-decadal trends in global terrestrial evapotranspiration and its components. *Scientific reports*, *6*(1), 1–12.

Supporting Information for "Causes of missing snowmelt following drought"

Dana A Lapides[1,2], W Jesse Hahm[2], Daniella M Rempe[3], John Whiting[1],

David N Dralle[1]

[1]Pacific Southwest Research Station, United States Forest Service, Davis, CA, USA

[2]Department of Geography, Simon Fraser University, Burnaby, BC, Canada

[3]University of Texas, Austin, Austin, TX, USA

Contents of this file

Introduction

This supplement contains supporting information, analyses, and figures for the study titled "Causes of missing snowmelt following drought."

Text S1. Site description and site selection

California experiences a Mediterranean climate with cool, wet winters and hot, dry summers. In much of California, wet season precipitation arrives as rain, but mountainous regions such as the Sierra Nevada predominantly receive snow. Mediterranean regions generally have highly variable annual precipitation (Langenbrunner et al., 2015) and are subject to rapid switches between drought and flood conditions (Horton et al., 2015; Dettinger et al., 2011). California has a particularly variable climate due to the added influence of complex topography (Swain et al., 2018). In the past decade, California has

experienced extreme drought (Griffin & Anchukaitis, 2014; Swain et al., 2016; Robeson, 2015) that resulted in extensive wildfires (Stephens et al., 2018; Diffenbaugh et al., 2015) and tree mortality (Fettig et al., 2019; Guarín & Taylor, 2005; Byer & Jin, 2017), and periods of extraordinarily high precipitation—e.g., winter 2016-2017 (Wang et al., 2017)—that resulted in widespread flooding (Wang et al., 2017) and landslides (Handwerger et al., 2019).

To explore drivers of low streamflow in 2021 in California, we examined a set of minimally disturbed, gauged watersheds in the Sierra Nevada (Figure 1c in main text). Sites were selected in the Sierra Nevada that met the following criteria:

1. no upstream dams (Falcone, 2017),

2. >20% precipitation falls as snow annually on average (Falcone, 2017),

3. watershed boundaries were delineated in NHD+ (Wieczorek, 2011),

4. <5% developed land cover (Homer et al., 2015),

5. <5% cultivated land cover (Homer et al., 2015),

6. <35% burned area between 1990 and 2020 (State of California and the Department of Forestry and Fire Protection, 2021),

7. <20% logged area from 1997-2018 (CAL FIRE, 2019),

8. at least 10 years with continuous streamflow from April 1 - September 1 (U.S. Geological Survey, 2021),

9. streamflow record includes 2021 (U.S. Geological Survey, 2021) or (Hunsaker & Safeeq, 2017).

All gages that met these criteria were reviewed manually to ensure hydrographs appear unmodified and snowmelt-dominated. We identified 15 catchments that met the selection criteria (Table S1), spread throughout the Sierra Nevada. Although P300 has a snow fraction of 19%, it is included to capture a larger range of sites. The sites encompass a range in size from 11 to 1,373 km^2, annual precipitation from 369 to 979 mm, and a mean streamflow from 0.3 to 190 m^3/s. 14 of 21 sites drain to the west, while the remaining sites (primarily those in the Tahoe area) drain to the east. Additionally, six basins essential to California's water supply were also included to demonstrate applicability of the presented methods to larger and more complex basins (bottom of Table S1).

Text S2. Detailed model description

(Hahm et al., 2019) developed a stochastic hydrological model incorporating root zone storage as a simple 1-d bucket that describes annual runoff dynamics in Mediterranean catchments. Similar to Figure 2 in the main text, the model describes a landscape with thin soil but a substantial weathered bedrock zone that stores plant-accessible water. The entire soil and weathered bedrock zone is treated as a single plant-accessible storage reservoir S [L]. During the wet season, precipitation P [L] contributes water to storage, and evapotranspiration ET [L] removes water from storage primarily during the dry season. Streamflow is generated only if the subsurface storage reservoir is full.

(Hahm et al., 2019), however, did not consider the scenario in which deficits were not replenished and could carry over between years. Evidence from field observations of soil and rock moisture and tree mortality (Goulden & Bales, 2019; Hahm et al., 2021) and from water balance approaches using satellite data products (McCormick et al., 2021; Wang-Erlandsson et al., 2016; Cui et al., 2022) shows that root zone storage deficits can

grow over multiple years, meaning that the deficit can vary substantially between years in a way that is important for vegetation response. Recent work also demosntrates that many hydrological models that lack the ability to generate multi-year deficits are unable to simulate streamflow conditions through multi-year droughts in Australia (Fowler et al., 2021). Changes in subsurface storage (and deficit) give watersheds "memory" of prior precipitation that can persist. More than 8 years after the Millennium Drought in southeastern Australia, many watersheds had not returned to pre-drought conditions (Peterson et al., 2021). They inferred that enhanced evaporation due to warmer conditions slowed recharge to the subsurface so that deficits generated during the Millennium Drought still were not satisfied. Thus, changes in ET can impact streamflow generation and also provide a feedback that strengthens the importance of subsurface storage deficit on streamflow.

Here, we extend the model presented by (Hahm et al., 2019) to allow for both multi-year deficit accrual and snow. To allow for multi-year deficit accrual, we explicitly track a timeseries of annual October 1 deficit so that initial water year conditions may vary between years, and to account for snow, we add a snowmelt period following the wet season (during which rain enters storage and snow accumulates), with the April 1 snowpack SWE [L] delivered at a rate of m [L/T]. (Hahm et al., 2019) assumed that cumulative wet season ET is constant from year to year, an assumption that was meant to reflect the fact that ET is energy-limited during the cold wet season in California. When considering the snowmelt period, though, ET total may not be constant between years since the length of the snowmelt period can vary substantially depending on the snowmelt rate m [L/T] and the size of the snowpack SWE. This dynamic can be accounted for in the

snowmelt period by considering ET during the melt period and post-snowmelt growing period as energy-determined rates ET_s [L/T] and ET_{summer} [L/T] that last for the duration of the melt period and summer respectively. Then, the total warm season $ET_{warm} = N_{melt}ET_s + N_{warm\_dry}ET_{summer}$ [L], where N_{melt} [T] and N_{warm_dry} [T] are the lengths of the melt period and post-snowmelt growing season, respectively.

Thus, the extended model includes three seasons with distinct fluxes: a winter wet season, a snowmelt period, and a snowmelt-free growing season:

$$S_{Apr1} = min(S_{max}, max(0, S_{Oct1} + P_w - ET_w)), \tag{1}$$

$$S_{Aug1} = min(S_{max}, max(0, S_{Apr1} + SWE - (ET_s - P_s)N_{melt})), \tag{2}$$

$$S_{Oct1} = max(0, S_{Aug1} - ET_{summer}N_{warm\_dry}), \tag{3}$$

where S_{Apr1} [L] is the root zone storage at the start of the snowmelt period, S_{Aug1} [L] is the root zone storage at the start of the post-snowmelt growing period, and S_{Oct1} [L] is the root zone storage at the start of the winter wet season. S_{max} [L] is the maximum possible value of root-zone storage, ET_w [L] is winter ET, and P_w [L] and P_s [L/T] are winter and spring rainfall. Because storage is constrained between 0 and S_{max}, ET cannot occur if storage is empty, and runoff is generated if storage is full, which can happen during the winter wet season or during the snowmelt period. Equation 1 describes the winter wet season when rain increases storage and ET draws from storage, Equation 2 the melt period when SWE melts into storage and a net ET flux draws from storage, and Equation 3 the post-melt growing season when ET draws from storage. For simplicity, we define a single term $ET_{net} = ET_s - P_s$ that describes the potential net ET during the melt period,

and ET_{summer} can be considered in the same way in regions with significant precipitation during the growing season.

By using the mass balance from Equations 1-3, streamflow during the snowmelt period is given by:

$$Q = \begin{cases} max(0, SWE - ET_{net}N_{melt}), & \text{if } P_w - ET_w > D_{Oct1} \\ max(0, SWE - ET_{net}N_{melt} - D_{Oct1} + (P_w - ET_w)), & \text{otherwise} \end{cases} \quad (4)$$

where Q [L] is total streamflow due to snowmelt, and D_{Oct1} [L] is the root zone storage deficit ($S_{max} - S_{Oct1}$) at the end of the preceding dry season. Both conditions are bounded by 0 since streamflow cannot be negative. A negative value for either condition indicates that water demand from ET exceeds water availability from rain, snowmelt, and storage, so streamflow must be 0.

In Equation 4, there are three terms that can cause the relationship between SWE and Q to be non-unique: (i) the total net ET flux during the melt period ($(ET_s - P_s)N_{melt}$), which is impacted indirectly by the melt rate m since $m = SWE/N_{melt}$, (ii) the root zone storage deficit at the end of the dry season D_{Oct1} (referred to as Oct. 1 deficit), which is driven by ET, precipitation, and runoff dynamics during prior years, and (iii) winter recharge ($P_w - ET_w$). Increasing total ET during the snowmelt period ($ET_{net}N_{melt}$) reduces streamflow generation. This ET term can be increased by increasing vegetation demand (increased ET_{net}), reducing spring rainfall (increased ET_{net}), or by slowing down the snowmelt rate m (increased length of N_{melt} for the same SWE). While increasing the October 1 deficit reduces streamflow generation, increasing winter recharge ($P_w - ET_w$) can increase streamflow generation. This can be achieved either by increasing P_w (decreasing annual snow fraction since SWE remains constant) or decreasing ET_w (reducing winter

ET), so long as storage is not already being filled up. See Supplemental Information S3 for a visual demonstration of how each parameter impacts Q. Any of these mechanisms could confound a linear regression model for streamflow based only on April 1 SWE.

Text S3. Concordance between PRISM and SNODAS

To confirm that SWE from SNODAS and precipitation from PRISM are compatible, we calculated annual snow fractions at each site using total daily increases in SWE and annual sum of PRISM. In essentially all cases, snow fraction was less than 1 (except for one year at site 10343500 when snow fraction was 1.06), and calculated mean snow fraction spanned a reasonable range at study sites (from 13% to 72%). Estimates of annual snow total were also made from a temperature threshold of 0°C using PRISM precipitation. Annual snowfall totals from SNODAS and estimated from PRISM were generally within 30-50% of one another, and the annual pattern of snow totals is generally consistent between these two estimates. Calculated snow fractions tend to be lower than literature reported values (e.g., $>$ 80% for 10343500), but there is evidence that snow fraction has decreased substantially through the period of record (Hatchett & McEvoy, 2018), and our snow fraction estimate is based only on the past 15 years. Additionally, since we believe that the patterns of snow and total precipitation are well-represented among these data sets, magnitude differences should not make a large difference in the results of this study since coefficients in a multiple linear regression adjust for magnitude errors. Only in the deficit calculation does the split between snow and precipitation matter. In these calculations, low estimates of snow relative to rain will mean that water is delivered to the root zone earlier in the year, potentially overestimating actual deficits generated in the warm season to a small degree.

Text S4. Subsurface deficit calculations

To estimate a storage deficit in the subsurface (D), we adapted the method presented by (Wang-Erlandsson et al., 2016) and updated to account for snow cover by (Dralle et al., 2021). In this method, root zone storage deficit is calculated as the running difference between fluxes leaving (F_{out} [L/T]) and entering (F_{in} [L/T]) the system during a time interval defined by the sampling frequency of remotely sensed products. Generally, F_{out} is set equal to ET, neglecting streamflow, and F_{in} is set equal to precipitation. Snow cover data from satellite products was perviously used to adjust fluxes in snow-dominated regions (Dralle et al., 2021). Here, since we have access to explicit information on snow through SNODAS (National Operational Hydrologic Remote Sensing Center, 2000), we incorporate snow directly into the mass balance approach by defining F_{in} as

$$F_{in} = P_r + Q_m, \tag{5}$$

where P_r is precipitation falling as rain determined as precipitation when SWE does not increase, and Q_m is given by decreases in SWE. More precisely,

$$P_{r,t_n} = P_{t_n} - \max(\mathrm{SWE}_{t_n} - \mathrm{SWE}_{t_{n-1}}, 0), \tag{6}$$

where P_i is the total precipitation falling in timestep i and SWE_i is the SWE at time step i and

$$Q_m = \max(\mathrm{SWE}_{t_{n-1}} - \mathrm{SWE}_{t_n}, 0). \tag{7}$$

Following the deficit tracking procedure presented by (Wang-Erlandsson et al., 2016), we proceed by calculating the difference between F_{out} and F_{in} over a time interval from

t_n to t_{n+1}:

$$A_{t_n \to t_{n+1}} = \int_{t_n}^{t_{n+1}} (F_{out} - F_{in})\, dt. \tag{8}$$

This accumulated difference ($A_{t_n \to t_{n+1}}$) is a *deficit*, so the signs of fluxes are reversed compared to a traditional mass balance. If the accumulated difference is negative, then no deficit has been accrued in the time step. So, a lower bound on root zone storage deficit for each time step is given by the maximum value of zero and the running sum of accumulated differences:

$$D(t_{n+1}) = \max(0, D(t_n) + A_{t_n \to t_{n+1}}) \tag{9}$$

Runoff is not needed to calculate accurate deficits

For multiple reasons, it is neither appropriate nor necessary to account for runoff in root-zone storage deficit calculations. First, water drainage from the root zone during precipitation or snowmelt can sustain streamflow production for weeks, even months, following the drainage event. This temporal mismatch between root-zone drainage and flow generation in the stream implies that any deficit generation related to flow production likely occurred well before the observation of flow; therefore, using streamflow in deficit calculations would increase deficits at the wrong time. One approach for accounting for runoff in deficit calculations might be to incorporate a root-zone drainage term, which is not straightforward to measure or estimate. However, this is not necessary as the drainage flux should have a minimal impact on deficit growth; significant drainage occurs primarily when the deficit is small or zero due to water inputs (snowmelt or precipitation). Further, this root-zone drainage flux is likely smaller than the water fluxes that generate drainage—as is accepted in modeling studies and suggested by findings of runoff ratios smaller than

1 in empirical studies (Botter et al., 2007; Rodriguez-Iturbe et al., 1999; Hunsaker et al., 2012)—meaning that the net change to the deficit would be negligible. Since the deficit is small or zero when drainage occurs, and inputs likely exceed the drainage flux, true deficit growth is unlikely to occur during drainage events. As a result, neglecting drainage in deficit calculations should not have a significant impact on calculated root-zone storage deficits.

Text S5. Factors that impact spring streamflow generation

As described in the main text, the relationship between April 1 SWE and spring streamflow is not unique. Within a mass balance framework, there are four factors that can drive lower spring streamflow: (a) more net spring ET (ET-rain), (b) a slower snowmelt rate, (c) a larger root zone storage deficit, or (d) less rainfall. Figure S1 uses the mass balance model to show directly how each of these four factors affects the resulting spring streamflow. For this exercise, we use this total ET_{warm} to set an average rate of ET during the warm season that is applied to both the snowmelt period and post-snowmelt growing season. We apply Equations 1-3 to track storage through time. Parameters S_{max}, ET_w, and $ET_{warm} = ET_s N_{melt} + ET_{summer} N_{warm\_dry}$ are the same each year, while P_w, P_s, SWE, and the partitioning of ET_{warm} between the snowmelt period and the snow-free growing season vary between years. A spinup period of 100 years is used to generate initial conditions. For each year, we select an annual precipitation from a gamma distribution. Since spring rainfall is included in the term ET_{net}, we do not explicitly include that rainfall in the annual precipitation. This simplification does not assume stationarity in spring rainfall but rather means that the annual precipitation total could be inaccurate if spring precipitation is significant. A future version of this model could include a

separate parameter to prescribe spring precipitation. Instead, we allow SWE and P_w to add to the gamma-selected annual precipitation, with the partition described by a fraction ($snowfrac$). This setup still results in a gamma distribution for annual precipitation since the spring rainfall is constant. Throughout the simulation period, we track storage deficits generated at the end of each growing season, SWE, and snowmelt runoff calculated for each year using Equation 4. Parameters used to generate the figure are in Table S3.

Text S6. Exploratory analysis of variables that impact melt period streamflow

We performed exploratory data analysis identify the importance of each variable that appears in Equation 4 for explaining residuals in snowpack-winter rainfall-runoff relationships. This analysis was used to select a minimal set of variables that both encompass all of the proposed mechanisms for failure of the SWE-Q model but minimizes correlation between variables. To do this, we wanted to select only one variable to represent each proposed mechanism. Exploratory analysis was used to find one variable for each mechanism that most strongly correlates with residuals in the SWE-Q model.

Figure S2g shows the time series of residuals in the April 1 SWE, winter rainfall - spring Q relationship (referred to hereafter as the SWE-Q relationship). Across all sites, 2021 generally stands out as the largest negative residual as a fraction of WY P (note reversed y-axis). See the data supplement to review residual timeseries for all study sites (Lapides et al., 2021). This finding indicates that less streamflow arrived than expected, and the missing streamflow was a substantial portion of the water budget. Based on the parsimonious model described in the main text, we explore four hypotheses to explain why 2021 spring streamflow was lower than expected at the 15 minimally impacted study sites. Results are shown in Figure S2 for Ward Creek (site 10336676), but results across

the study sites are qualitatively similar, see data supplement (Lapides et al., 2021). We selected Ward Creek since it has the highest-performing multiple linear regression model but is otherwise representative of the trends and site characteristics across the study sites.

Hypothesis 1: ET was larger than usual

Spring net ET was unusually high

In 2021, spring ET was lower than usual (Figure S2b) despite high spring temperatures (Figure S2a). The Evaporative Stress Index (ESI) data indicate that plants were water-stressed in 2021 (Figure S2b). While ET was not higher than usual, spring ET accounted for a larger fraction of the annual water budget than usual since annual precipitation was very low (Figure S2a). However, spring ET alone does not explain the magnitude of the residual from the SWE-Q relationship in 2021. Spring ET / WY P explains only 20% of variance in the residuals at Ward Creek (Figure S2i), compared to 7% explained just by WY P (Figure S2h). Over all sites, the median NSE is 16% for Spring ET / WY P.

Spring rain accounted for a much smaller fraction of annual precipitation than usual in 2021, about half of the median (Figure S2c). As with spring ET in 2021, though, spring P fraction was not outside the range of previously observed values at most sites.

Since net spring ET (ET_{net}) is defined as the difference between spring ET and spring rain, the deviations in the individual terms are combined in ET_{net}. Neither spring ET nor spring rain were outside the range observed in prior years, but ET_{net} was unprecedented in 2021 (red scatter point in Figure S2j). ET_{net} both singles out 2021 as a unique year and explains 62% of variance in the residuals at Ward Creek (Figure S2j). Across all sites, the median R^2 value between residuals and ET_{net} is 0.26, and ET_{net} only singles out 2021 at 2 sites of 15.

Winter recharge was unusually low

Winter recharge is controlled by the offset between winter rainfall and winter ET. Winter rainfall is included in the original forecast model. The other factor controlling winter recharge is winter ET. While spring ET was low in the 2021 WY, this was not the case for winter ET, which was higher than normal (Figure S2d). As with ET_{net}, $(ET_w - P_w)$ / WY P singles out 2021 as a particularly extreme year (Figure S2k) with the highest relative ET_w in the study period, an observation that holds for 5 of the 15 study sites, and accounts for 15% of variance in the residuals at Ward Creek. Across all study sites the median variance explained is 2%.

Hypothesis 2: Melt rate was unusually slow

By examining Figure S2e, it is clear that the melt rate in 2021 was slower than usual at Ward Creek, among the slowest melt rates observed in the time period 2003-2021, although not outside the previously observed range. A slow melt rate can reduce streamflow by allowing plants to take greater advantage of snowmelt for ET, which means that it is not melt rate alone but its ratio to ET_{net} that drives the impact of melt rate on streamflow generation, since $m = SWE/N_{melt}$ (see Equation 4). In 2021, the ratio m/ET_{net} was the smallest observed during the study period, and it explains 46% of the variance in the residuals at Ward Creek (Figure S2l). At all other study sites, though, m/ET_{net} generally explains less than 2% of variance for most sites, with a median of 1%.

Hypothesis 3: Root zone storage deficit was unusually large

Each year, the root zone storage deficit grows during the dry season and shrinks during the wet season (black line in Figure S2f). The maximum deficit each year (red dots,

estimated by October 1 deficit for all analyses for simplicity), provides information about how much water was removed from storage during the preceding dry season(s) by ET. Note that the October 1 deficit is always larger than the soil water storage capacity, indicating that plants access water stored in weathered bedrock. The minimum deficit each year (yellow dots) provides information about wet season replenishment of root zone storage. For Ward Creek shown in Figure S2f, the minimum deficit is always 0, but it can be nonzero and even grow across multiple years at other sites—see the data supplement for study sites that demonstrate deficit carry-over between years (Lapides et al., 2021). In 2021, a large deficit was generated—among the largest during the study period. As with the other hypothesis variables, though, the significance of the 2021 deficit is much clearer when compared to the annual water budget. Figure S2m shows that the deficit as a fraction of the annual precipitation was more than 50% larger than the largest observed value in previous years. Thus, the deficit strongly identifies 2021 as an outlier, consistent with observations of substantial missing streamflow, and the root zone storage deficit explains 57% of the variance in residuals in the SWE-Q relationship at Ward Creek. At 12 of 15 study sites, the October 1 deficit in 2021 was the largest or second-largest deficit recorded in the study period (as a fraction of WY P). Median R^2 across minimally disturbed study sites is 0.24.

These exploratory analyses motivated the choice of variables included in the multiple linear regression model. The outcomes of the multiple linear regression are summarized in Table S5 for (top) wet years and (bottom) dry years. Performance comparison between different linear regression models is in Table S7, including performance for wet/dry year model parameters shown in Table S5.

Text S7. A random forest model for spring streamflow

In this study, we developed a multiple linear regression model for each study site to explain spring streamflow production from snowmelt. However, while the model presented in the main text shows linear relationships among all variables for idealized catchments, the relationships between each investigated variable may not be linear for real catchments. To capture more complex relationships among the variables, we also developed a random forest model, using the same set of variables described in Table 1 in the main text. Since random forest models are data-driven and flexible, we chose to train a single random forest model using data from all sites. Performance of the random forest model was exceptional (Figure S3a, NSE=0.98, see Table S4 for site-specific performance), and feature importance (Figure S3b) supports similar conclusions to the effect size results using the multiple linear regression model. The exact ordering of feature importance is not identical to the ordering implied by the multiple linear regression, but both models support the conclusion that the melt rate does not provide much predictive power, and the deficit provides a substantial amount of predictive power (Figure S3b). Partial dependence plots (Figure S3c-h) shows the functional form of the learned relationship between each variable and the output (spring streamflow). These functional forms are nearly monotonic, with small deviations from monotonic behavior likely due to co-variability of variables with parameters not included in the model. In all cases, the general direction of the relationship matches our hypotheses in the main text: (c) higher SWE results in higher streamflow, (d) larger deficit results in smaller streamflow, (e) more spring ET results in less streamflow, (f) a faster melt rate results in more streamflow, (g) more rainfall results in more streamflow, and (h) less winter ET results in more streamflow. Insets show the raw data used to train

the model. For the most predictive variables, the learned relationship is clearly visible in scatter plots of raw data as well, providing additional confidence in the results.

Text S8. Additional details on multiple linear regression models

Tables S5-S7 show effect sizes for multiple linear regression models at all sites and show site-specific performance of different regression models both overall and on years following wet or dry years separately.

Text S9. Calculated deficit is driven by root-zone water use

The mass balance approach applied to calculate the storage deficit relies on distributed products. We claim that the balance represents processes in the root-zone; however it is also possible that evaporation from upwelling groundwater and surface water sources contribute to observed ET and thus the storage dynamic calculated. This effect, however, is negligible. To demonstrate this, we assumed a maximal surface water coverage area from which this evaporation could occur by using the NHDPlus stream network for each USGS gage and a furthest downstream (gage location) estimate of stream width from Google Earth Pro. We then estimated annual PET from surface water bodies in each watershed by multiplying mean total MODIS PET by the maximum surface water coverage in the watershed (Table S8). Even with absurdly large stream width estimates applied to the full channel network (a headwater stream is not 30 m wide), none of the size have the possibility of more that 15% of ET going to surface water evaporation, and it is very likely that ¡1% of evaporative can be attributed to surface water sources.

References

Botter, G., Porporato, A., Daly, E., Rodriguez-Iturbe, I., & Rinaldo, A. (2007). Prob-

abilistic characterization of base flows in river basins: Roles of soil, vegetation, and geomorphology. *Water Resources Research*, *43*(6).

Byer, S., & Jin, Y. (2017). Detecting drought-induced tree mortality in sierra nevada forests with time series of satellite data. *Remote Sensing*, *9*(9), 929.

CAL FIRE. (2019). *Timber harvest plans (THPs) - CAL FIRE [ds816].*

Cui, G., Ma, Q., & Bales, R. (2022). Assessing multi-year-drought vulnerability in dense mediterranean-climate forests using water-balance-based indicators. *Journal of Hydrology*, 127431.

Dettinger, M. D., Ralph, F. M., Das, T., Neiman, P. J., & Cayan, D. R. (2011). Atmospheric rivers, floods and the water resources of california. *Water*, *3*(2), 445–478.

Diffenbaugh, N. S., Swain, D. L., & Touma, D. (2015). Anthropogenic warming has increased drought risk in california. *Proceedings of the National Academy of Sciences*, *112*(13), 3931–3936.

Dralle, D. N., Hahm, W. J., Chadwick, K. D., McCormick, E., & Rempe, D. M. (2021). Accounting for snow in the estimation of root zone water storage capacity from precipitation and evapotranspiration fluxes. *Hydrology and Earth System Sciences*, *25*(5), 2861–2867.

Falcone, J. (2017). Us geological survey gages-ii time series data from consistent sources of land use, water use, agriculture, timber activities, dam removals, and other historical anthropogenic influences: Us geological survey data release. In *Us geological survey data release.*

Fettig, C. J., Mortenson, L. A., Bulaon, B. M., & Foulk, P. B. (2019). Tree mortality following drought in the central and southern sierra nevada, california, us. *Forest*

Ecology and Management, *432*, 164–178.

Fowler, K. J., Coxon, G., Freer, J. E., Knoben, W. J., Peel, M. C., Wagener, T., ... Zhang, L. (2021). Towards more realistic runoff projections by removing limits on simulated soil moisture deficit. *Journal of Hydrology*, *600*, 126505.

Goulden, M. L., & Bales, R. C. (2019). California forest die-off linked to multi-year deep soil drying in 2012–2015 drought. *Nature Geoscience*, *12*(8), 632–637.

Griffin, D., & Anchukaitis, K. J. (2014). How unusual is the 2012–2014 california drought? *Geophysical Research Letters*, *41*(24), 9017–9023.

Guarín, A., & Taylor, A. H. (2005). Drought triggered tree mortality in mixed conifer forests in yosemite national park, california, usa. *Forest ecology and management*, *218*(1-3), 229–244.

Hahm, W. J., Dralle, D., Rempe, D., Bryk, A., Thompson, S., Dawson, T., & Dietrich, W. (2019). Low subsurface water storage capacity relative to annual rainfall decouples mediterranean plant productivity and water use from rainfall variability. *Geophysical Research Letters*, *46*(12), 6544–6553.

Hahm, W. J., Dralle, D. N., Sanders, M., Bryk, A. B., Fauria, K. E., Huang, M.-H., ... others (2021). Bedrock vadose zone storage dynamics under extreme drought: consequences for plant water availability, recharge, and runoff. *ESSOAR Pre-Print (https://www.essoar.org/doi/abs/10.1002/essoar.10509661.2)*.

Handwerger, A. L., Fielding, E. J., Huang, M.-H., Bennett, G. L., Liang, C., & Schulz, W. H. (2019). Widespread initiation, reactivation, and acceleration of landslides in the northern california coast ranges due to extreme rainfall. *Journal of Geophysical Research: Earth Surface*, *124*(7), 1782–1797.

Hatchett, B. J., & McEvoy, D. J. (2018). Exploring the origins of snow drought in the northern sierra nevada, california. *Earth Interactions*, *22*(2), 1–13.

Homer, C., Dewitz, J., Yang, L., Jin, S., Danielson, P., Xian, G., ... Megown, K. (2015). Completion of the 2011 national land cover database for the conterminous united states–representing a decade of land cover change information. *Photogrammetric Engineering & Remote Sensing*, *81*(5), 345–354.

Horton, D. E., Johnson, N. C., Singh, D., Swain, D. L., Rajaratnam, B., & Diffenbaugh, N. S. (2015). Contribution of changes in atmospheric circulation patterns to extreme temperature trends. *Nature*, *522*(7557), 465–469.

Hunsaker, C. T., & Safeeq, M. (2017). Kings river experimental watersheds stream discharge.
doi: 10.2737/RDS-2017-0037

Hunsaker, C. T., Whitaker, T. W., & Bales, R. C. (2012). Snowmelt runoff and water yield along elevation and temperature gradients in california's southern sierra nevada 1. *JAWRA Journal of the American Water Resources Association*, *48*(4), 667–678.

Langenbrunner, B., Neelin, J. D., Lintner, B. R., & Anderson, B. T. (2015). Patterns of precipitation change and climatological uncertainty among cmip5 models, with a focus on the midlatitude pacific storm track. *Journal of Climate*, *28*(19), 7857–7872.

Lapides, D. A., Hahm, W. J., Rempe, D. M., & Dralle, D. N. (2021). *Supplementary code and data for: Root zone storage deficits mediate the production of streamflow from snowmelt.* (accessed at `https://github.com/lapidesd/CA\_missing\_freshet`)
doi: 10.5281/zenodo.6144807

McCormick, E. L., Dralle, D. N., Hahm, W. J., Tune, A. K., Schmidt, L. M., Chadwick, K. D., & Rempe, D. M. (2021). Widespread woody plant use of water stored in bedrock. *Nature*, *597*(7875), 225–229.

National Operational Hydrologic Remote Sensing Center. (2000). *Snow data assimilation system (snodas) data products at nsidc, version 1.* Boulder, Colorado USA. NSIDC: National Snow and Ice Data Center. doi: \url{https://doi.org/10.7265/N5TB14TC}

Peterson, T. J., Saft, M., Peel, M., & John, A. (2021). Watersheds may not recover from drought. *Science*, *372*(6543), 745–749.

Robeson, S. M. (2015). Revisiting the recent california drought as an extreme value. *Geophysical Research Letters*, *42*(16), 6771–6779.

Rodriguez-Iturbe, I., Porporato, A., Ridolfi, L., Isham, V., & Coxi, D. (1999). Probabilistic modelling of water balance at a point: the role of climate, soil and vegetation. *Proceedings of the Royal Society of London. Series A: Mathematical, Physical and Engineering Sciences*, *455*(1990), 3789–3805.

State of California and the Department of Forestry and Fire Protection. (2021). *Fire perimeters through 2020.*

Stephens, S. L., Collins, B. M., Fettig, C. J., Finney, M. A., Hoffman, C. M., Knapp, E. E., ... Wayman, R. B. (2018). Drought, tree mortality, and wildfire in forests adapted to frequent fire. *BioScience*, *68*(2), 77–88.

Swain, D. L., Horton, D. E., Singh, D., & Diffenbaugh, N. S. (2016). Trends in atmospheric patterns conducive to seasonal precipitation and temperature extremes in california. *Science Advances*, *2*(4), e1501344.

Swain, D. L., Langenbrunner, B., Neelin, J. D., & Hall, A. (2018). Increasing precipitation volatility in twenty-first-century california. *Nature Climate Change*, *8*(5), 427–433.

U.S. Geological Survey. (2021). *National water information system data available on the world wide web (water data for the nation).* (accessed December 2021)

Wang, S.-Y. S., Yoon, J.-H., Becker, E., & Gillies, R. (2017). California from drought to deluge. *Nature Climate Change*, *7*(7), 465–468.

Wang-Erlandsson, L., Bastiaanssen, W. G., Gao, H., Jägermeyr, J., Senay, G. B., Van Dijk, A. I., ... Savenije, H. H. (2016). Global root zone storage capacity from satellite-based evaporation. *Hydrology and Earth System Sciences*, *20*(4), 1459–1481.

Wieczorek, M. (2011). *USGS Streamgage NHDPlus Version 1 Basins 2011.*

Table S1. Catchment attributes for study sites. Streamflow and basic site information are from NWIS (U.S. Geological Survey, 2021), and climate information are derived from GAGES-II (Falcone, 2017).

Site	Stream name	Gage location	Area [km^2]	MAP [mm]	Snow %	Mean Ann. Q [mm]
Minimally disturbed basins:						
10336780	Trout Creek	-119.972, 38.9199	95	893	67	315
10336645	General Creek	-120.118, 39.0518	19	1202	58	740
10336660	Blackwood Creek	-120.162, 39.1074	29	1486	59	1018
10336676	Ward Creek	-120.157, 39.1321	25	1549	61	885
10343500	Sagehen Creek	-120.237, 39.4315	27	976	65	319
10308783	Leviathan Creek	-119.656, 38.7012	11	635	60	50
11383500	Deer Creek	-121.948, 40.0140	539	1484	32	499
11189500	SF Kern River	-118.173, 35.7374	1373	477	36	72
11204100	SF Tule River near Reservation	-118.813, 36.0241	248	798	25	128
11203580	SF Tule River near Cholollo Camp	-118.654, 36.0482	52	996	44	278
11266500	Merced River at Pohono Bridge	-119.666, 37.7168	831	1213	60	685
11264500	Merced River at Happy Isles Bridge	-119.558, 37.7315	469	1199	68	673
10265150	Hot Creek	-118.817, 37.6688	177	814	72	262
P300	Providence	-119.204, 37.0538	5	880	19	360
B200	Bull	-119.083, 36.9790	5	946	45	422
Basins essential for California water supply:						
11525500	Trinity River	-122.804, 40.7193	1862	1445	17	405
11377100	Sacramento River	-122.187, 40.2885	23051	972	27	426
11270900	Merced River	-120.332, 37.5216	2748	1032	29	399
11289650	Tuolumne River	-120.442, 37.6663	3983	1098	37	222
11319500	Mokelumne River below Merced Falls	-120.720, 38.3127	1408	1265	38	612
11335000	Cosumnes River	-121.045, 38.5002	1388	1073	13	292

Table S2. Table of notation.

Variable	Dimensions	Description
Q	L	Total runoff during snowmelt period
SWE	L	Snowpack at start of snowmelt period
P	L	Water year total precipitation
m	L/T	Snowmelt rate
ET_s	L/T	Mean spring ET rate
ET_w	L	Total winter ET
P_s	L/T	Mean spring rainfall rate
P_w	L	Total winter rainfall
ET_{net}	L/T	Spring ET rate - spring rainfall rate
N_{melt}	T	Duration of snowmelt period
D_{oct1}	L	Deficit at start of wet season

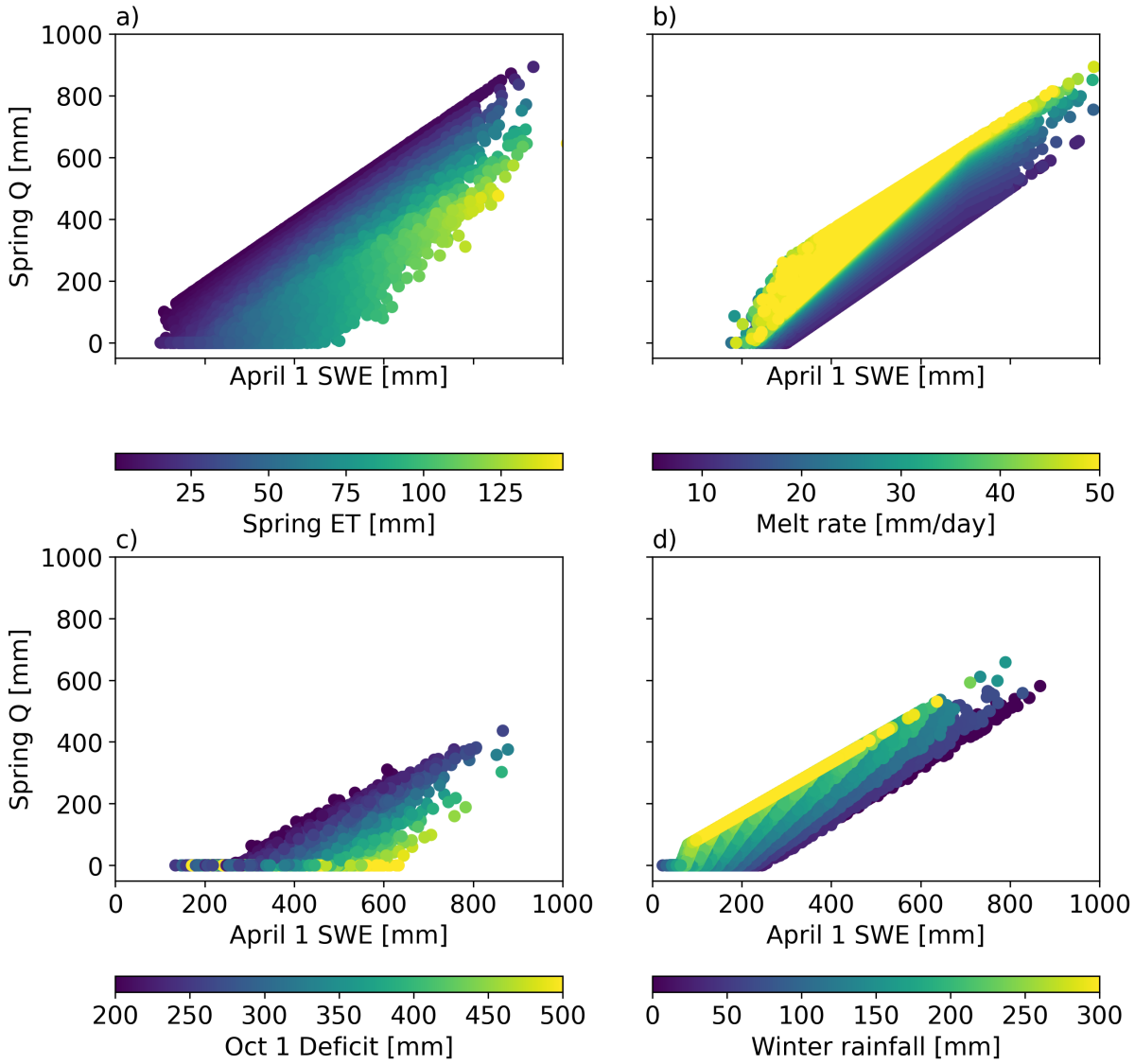

Figure S1. Differences in (a) spring evapotranspiration (ET), (b) snow melt rate, (c) root zone storage deficit, and (d) winter rainfall can result in different spring streamflow from the same April 1 SWE, as shown by Monte Carlo simulations with annual precipitation P selected from a gamma distribution and April 1 SWE given as a fraction of P. Parameters used to generate this figure are shown in Table S3. Melt rate is calculated assuming a 180 day warm season.

Table S3. Parameter values used to generated each subfigure in Figure S1: S_{max} is maximum root zone storage; PET is total potential evapotranspiration in the warm season; ET_w in the winter; μ and sd are parameters for the gamma distribution for annual precipitation; snowfrac is the fraction of annual precipitation that falls as snow; and m is the snowmelt rate.

Panel	S_{max}	ET_{warm}	ET_w	μ	sd	snowfrac	m
a	1,000	10-300	0	400	100	1	10
b	300	800	0	700	150	0.7	10-50
c	1,000	350	0	400	100	1	10
d	300	300	0	400	100	0.25-1	10

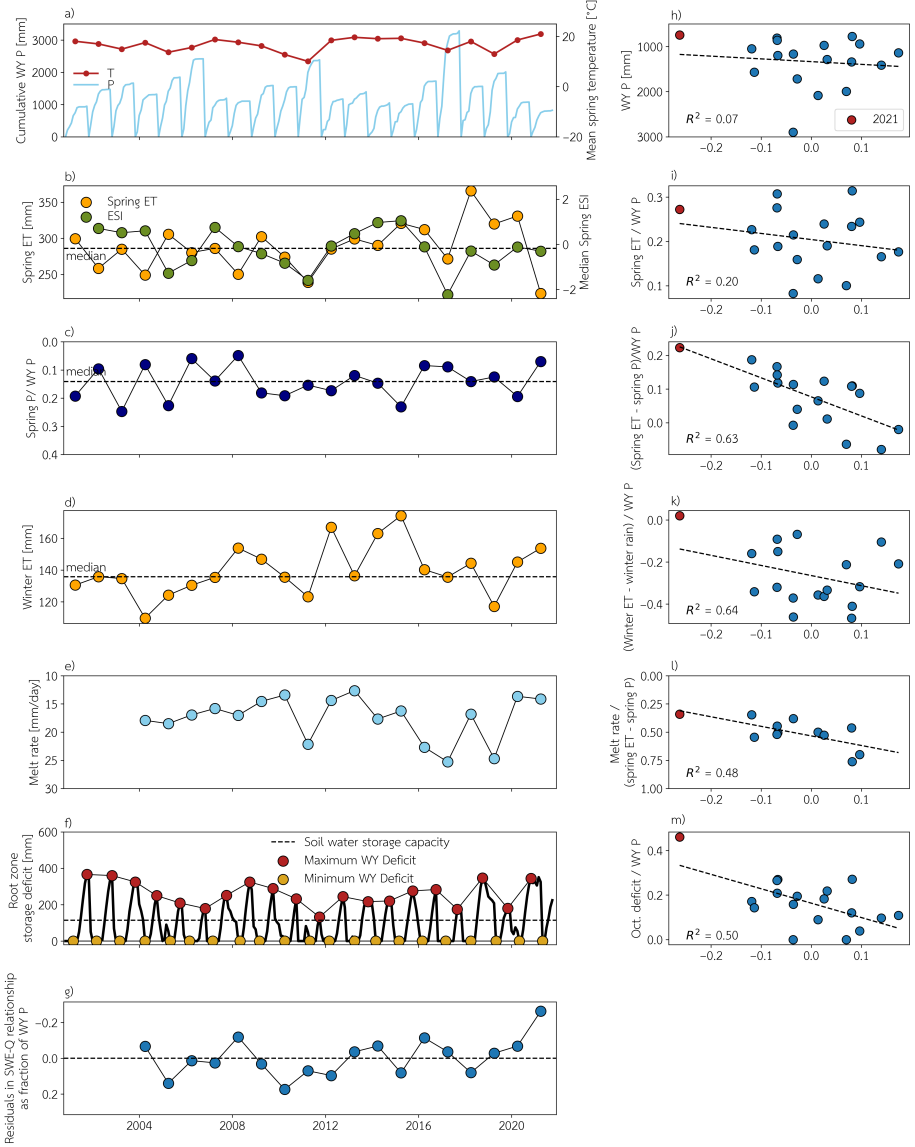

Figure S2. Water year data for one representative study site (Ward Ck). Spring ET and spring P are for the months April-July. All panels are oriented so that moving vertically in the panel theoretically results in less spring streamflow. In particular, note that the y-axes for panels c, e, h, i, and m and the x-axis for panels g-k are reversed. As a result, all relationships in panels g-k should appear negative. Red scatter points in panels g-k mark the 2021 water year.

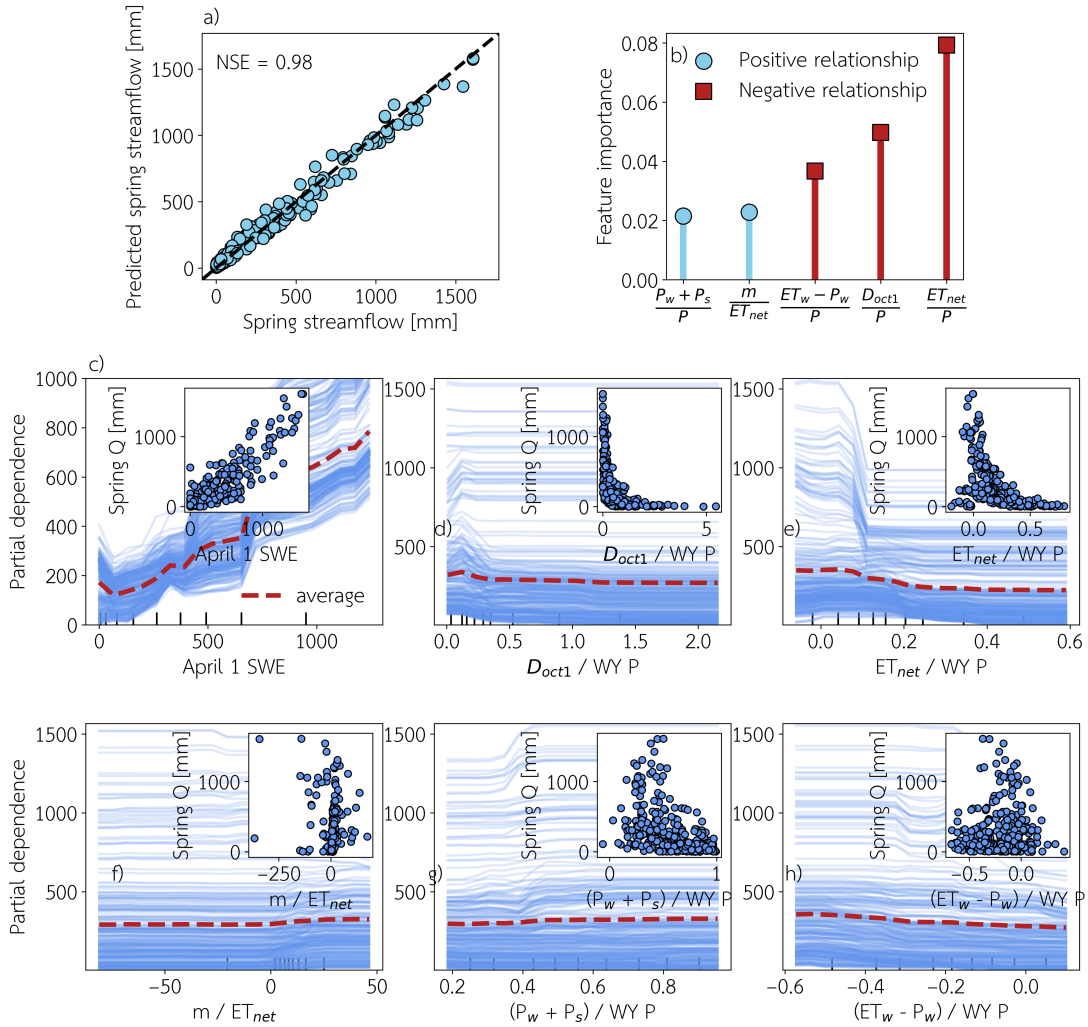

Figure S3. (a) Performance of random forest model for spring streamflow trained for all study sites. (b) Feature importance for parameters included in random forest model, except for April 1 SWE, which is significantly more important than all other parameters. (c)-(h) are partial dependence plots with the average partial dependence shown as a red dashed line. Panels (d)-(e) are zoomed in, which excludes some of the blue lines but allows for the functional shape of the relationships to be more clearly seen. For comparison, scatter data for the relationship between each parameter and measured spring streamflow is shown as an inset to each subplot.

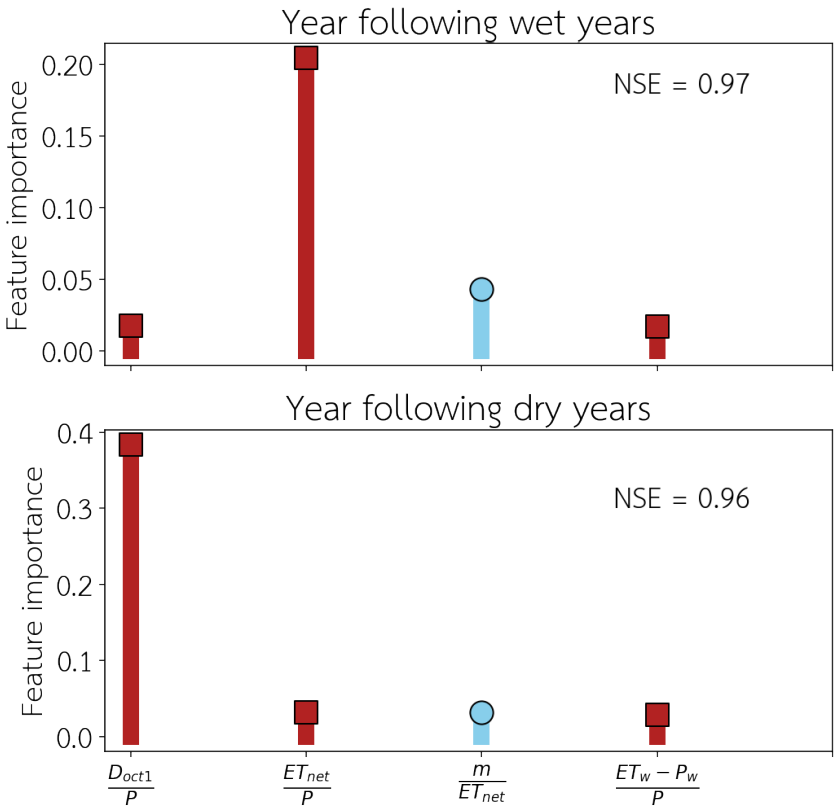

Figure S4. Feature importance for a random forest model trained across all sites in (a) years following wet years and (b) years following dry years.

Table S4. Site-specific performance of random forest model.

Site	NSE
10336780	0.94
10336645	0.96
10336660	0.96
10336676	0.99
10343500	0.87
10308783	0.67
11383500	0.85
11189500	0.96
11204100	0.94
11203580	0.96
11266500	0.98
11264500	0.99
10265150	0.13
P300	0.90
B200	0.94

Table S5. Parameters for the multiple linear regression model to predict spring streamflow. For parameter descriptions, see Table 1 in the main text. Parameter values are shown multiplied by median absolute variable values among (top) top 25th percentile wettest years and (below) driest 25th percentile of water years and shown in units of mm for comparison. Values marked by an asterisk indicate that the sign is opposite to the expected sign based on hypothesized mechanisms. Parameter columns are listed in order of decreasing median effect size, so SWE has the largest effect size, and m/ET_{net} the smallest across the study sites. Normalized parameters are shown in Table S6.

Site	SWE	P_w	$\frac{D_{Oct1}}{P}$	$\frac{ET_{net}N_{melt}}{P}$	$\frac{ET_w - P_w}{P}$	$\frac{m}{ET_{net}}$
Years following wet years						
10336780	176	125	-38	5*	-2	0
10336645	369	106	-50	-20	-38	-6*
10336660	410	27	-111	-76	-193	7
10336676	428	211	-100	-69	-84	2
10343500	265	75	-58	1*	-34	-31*
10308783	13	19	-34	-64	-4	24
11383500	37	221	-54	-39	-58	-1*
11189500	23	-33*	-0	-20	-6	8
11204100	7	219	-17	-52	6*	1
11203580	24	168	-24	-78	-24	4
11266500	288	85	-61	-42	-29	15
11264500	277	116	-50	-40	-1	7
10265150	16	7	-18	-32	-7	1
P300	4	-8*	-45	-138	-80	11
B200	15	-265*	25*	-221	-48	27
Median	37	86	-45	-42	-29	4
Years following dry years						
10336780	258	105	-62	3*	-12	0
10336645	423	64	-95	-18	-13	-7*
10336660	512	24	-202	-45	-156	10
10336676	573	192	-190	-34	-80	3
10343500	285	63	-82	1	-12	-31*
10308783	13	19	-52	-41	-4	27
11383500	63	209	-47	-48	-71	-1*
11189500	16	-33*	-1	-20	-2	6
11204100	3	227	-42	-79	6*	0
11203580	9	186	-57	-122	-22	2
11266500	396	73	-105	-29	-41	17
11264500	391	95	-89	-25	-7	10
10265150	22	7	-58	-21	-1	1
P300	0	-8*	-93	-170	-68	8
B200	3	-338*	56*	-257	-52	30
Median	63	64	-62	-34	-12	3

Table S6. Parameters for the multiple linear regression model to predict spring streamflow. For parameter descriptions, see Table 1 in the main text. Here, parameter values from Table S5 are normalized so that the sum of the absolute value of each row is 1.

Site	SWE	P_w	$\frac{D_{Oct1}}{P}$	$\frac{ET_{net}N_{melt}}{P}$	$\frac{ET_w - P_w}{P}$	$\frac{m}{ET_{net}}$
Years following wet years						
10336780	0.51	0.36	-0.11	0.01*	-0.00	-0.00*
10336645	0.63	0.18	-0.08	-0.03	-0.06	-0.01*
10336660	0.50	0.03	-0.13	-0.09	-0.23	0.00
10336676	0.48	0.24	-0.11	-0.08	-0.09	0.00
10343500	0.57	0.16	-0.13	0.00	-0.07	-0.07*
10308783	0.08	0.12	-0.22	-0.40	-0.02	0.15
11383500	0.09	0.54	-0.13	-0.10	-0.14	-0.00*
11189500	0.25	-0.37*	-0.00	-0.22	-0.07	0.09
11204100	0.02	0.73	-0.05	-0.17	0.02*	0.00
11203580	0.07	0.52	-0.08	-0.24	-0.07	0.01
11266500	0.55	0.16	-0.12	-0.08	-0.06	0.03
11264500	0.56	0.24	-0.10	-0.08	-0.00	0.01
10265150	0.19	0.09	-0.22	-0.40	-0.01	0.01
P300	0.01	-0.03*	-0.16	-0.48	-0.28	0.04
B200	0.02	-0.44*	0.04*	-0.37	-0.08	0.04
Median	0.24	0.16	-0.11	-0.09	-0.07	0.01
Years following dry years						
10336780	0.59	0.24	-0.14	0.0*	-0.03	-0.00*
10336645	0.68	0.10	-0.15	-0.03	-0.02	-0.01*
10336660	0.54	0.02	-0.21	-0.05	-0.16	0.01
10336676	0.53	0.18	-0.18	-0.03	-0.07	0.00
10343500	0.60	0.13	-0.17	0.00	-0.02	-0.06*
10308783	0.08	0.12	-0.33	-0.26	-0.03	0.17
11383500	0.14	0.48	-0.11	-0.11	-0.16	-0.00*
11189500	0.20	-0.42*	-0.01	-0.26	-0.03	0.08
11204100	0.01	0.64	-0.11	-0.22	0.02*	0.00
11203580	0.02	0.47	-0.14	-0.31	-0.06	0.00
11266500	0.60	0.11	-0.16	-0.04	-0.06	0.03
11264500	0.63	0.15	-0.15	-0.04	-0.01	0.01
10265150	0.20	0.07	-0.53	-0.19	-0.01	0.01
P300	0.00	-0.02*	-0.27	-0.49	-0.20	0.02
B200	0.00	-0.46*	0.08*	-0.35	-0.07	0.04
Median	0.20	0.12	-0.15	-0.11	-0.03	0.01

Table S7. Performance of the multiple linear regression model to predict spring streamflow. For parameter descriptions, see Table 1 in the main text. NSE values are shown for full model, a model using only April 1 SWE and D_{Oct1} / Winter P as variables, and a model only using April 1 SWE. The latter two models can both be run prior to snowmelt. The final two columns compare the NSE value for a regression model using only April 1 SWE on the years following the top 25th percentile years versus the bottom 25th percentile of years in terms of annual precipitation. NSE_{wet} and NSE_{dry} refer to the NSE for years following wet and dry years, respectively.

Site	NSE (all param)	NSE_{wet}	NSE_{dry}	NSE (SWE, $\frac{D_{Oct1}}{P_w}$)	NSE_{wet}	NSE_{dry}	NSE (SWE, P_w)	NSE_{wet}	NSE_{dry}
10336780	0.94	0.93	0.82	0.90	0.98	0.66	0.94	0.91	0.64
10336645	0.93	0.91	0.72	0.90	0.78	0.63	0.89	0.85	0.51
10336660	0.96	0.91	0.90	0.93	0.70	0.89	0.91	0.98	0.71
10336676	0.98	0.94	0.93	0.95	0.82	0.87	0.93	0.97	0.76
10343500	0.98	0.94	0.90	0.79	-0.27	0.50	0.96	0.98	0.75
10308783	0.87	0.83	0.59	0.64	0.85	-0.34	0.91	0.93	0.42
11383500	0.78	0.76	-1.83	0.58	0.55	0.02	0.81	0.89	0.18
11189500	0.87	0.90	0.28	0.75	0.88	0.20	0.89	0.92	-0.21
11204100	0.91	0.94	0.55	0.72	0.13	0.64	0.80	-0.13	0.18
11203580	0.92	0.86	0.64	0.73	0.07	0.72	0.89	0.65	0.42
11266500	0.96	0.80	0.98	0.92	0.64	0.91	0.95	0.84	0.98
11264500	0.93	0.67	0.94	0.90	0.42	0.94	0.92	0.71	0.96
10265150	0.81	0.68	0.42	0.71	0.01	0.47	0.82	0.23	0.24
P300	0.75	0.67	0.23	0.50	-2.42	0.35	0.85	0.71	-0.10
B200	0.90	0.49	0.97	0.76	0.34	-0.34	0.77	0.27	-1.29
Median	0.92	0.86	0.72	0.79	0.55	0.62	0.89	0.85	0.42

Site	Channel length [km]	Bankfull width at gage [m]	Mean Annual ET [mm]	Mean Annual ET [km^3]	Max. PET from surface water [km^3]	% of ET
10336780	102	5	543	0.0516	0.0011	2
10336645	23	4	580	0.0110	0.0002	2
10336660	28	4	573	0.0166	0.0002	1
10336676	14	3	577	0.0144	0.0001	1
10343500	28	3	597	0.0161	0.0002	1
10308783	8	5	525	0.0058	0.0001	2
11383500	436	15	635	0.3424	0.0141	4
11189500	1073	10	404	0.5548	0.0292	5
11204100	228	11	716	0.1777	0.0065	4
11203580	54	11	782	0.0407	0.0015	4
11266500	777	30	437	0.3628	0.0528	15
11264500	459	22	400	0.1877	0.0229	12
10265150	116	17	373	0.06609	0.0046	7

Table S8. Comparison between mean annual ET from PML-V2 and maximum PET from surface water bodies at each USGS site. See text for a description of how maximum PET from surface water bodies was calculated. Channel length is the tributary length from PyNHD (`https://pypi.org/project/pynhd/`). Stream widths were measured remotely at the gage location using Google Earth.